CORE
Metadata, citation and similar papers at core.ac.uk
Provided by Elsevier - Publisher Connector

Biochimica et Biophysica Acta 1857 (2016) 46–59

Contents lists available at ScienceDirect

Biochimica et Biophysica Acta

journal homepage: www.elsevier.com/locate/bbabio

Characterization of thylakoid membrane in a heterocystous cyanobacterium and green alga with dual-detector fluorescence lifetime imaging microscopy with a systematic change of incident laser power

Shuho Nozue [a], Akira Mukuno [a], Yumi Tsuda [a], Takashi Shiina [b], Masahide Terazima [a], Shigeichi Kumazaki [a,*]

[a] Department of Chemistry, Graduate School of Science, Kyoto University, Kyoto 606-8502, Japan
[b] Graduate School of Life and Environmental Sciences, Kyoto Prefectural University, Sakyo-ku, Kyoto 606-8522, Japan

ARTICLE INFO

Article history:
Received 3 June 2015
Received in revised form 29 September 2015
Accepted 11 October 2015
Available online 22 October 2015

Keywords:
Photosystem II
Photosystem I
Chlorophyll fluorescence
Fluorescence lifetime imaging microscopy
Heterocystous cyanobacteria
Green algae

ABSTRACT

Fluorescence Lifetime Imaging Microscopy (FLIM) has been applied to plants, algae and cyanobacteria, in which excitation laser conditions affect the chlorophyll fluorescence lifetime due to several mechanisms. However, the dependence of FLIM data on input laser power has not been quantitatively explained by absolute excitation probabilities under actual imaging conditions. In an effort to distinguish between photosystem I and photosystem II (PSI and PSII) in microscopic images, we have obtained dependence of FLIM data on input laser power from a filamentous cyanobacterium *Anabaena variabilis* and single cellular green alga *Parachlorella kessleri*. Nitrogen-fixing cells in *A. variabilis*, heterocysts, are mostly visualized as cells in which short-lived fluorescence (≤0.1 ns) characteristic of PSI is predominant. The other cells in *A. variabilis* (vegetative cells) and *P. kessleri* cells show a transition in the status of PSII from an open state with the maximal charge separation rate at a weak excitation limit to a closed state in which charge separation is temporarily prohibited by previous excitation(s) at a relatively high laser power. This transition is successfully reproduced by a computer simulation with a high fidelity to the actual imaging conditions. More details in the fluorescence from heterocysts were examined to assess possible functions of PSII in the anaerobic environment inside the heterocysts for the nitrogen-fixing enzyme, nitrogenase. Photochemically active PSII:PSI ratio in heterocysts is tentatively estimated to be typically below our detection limit or at most about 5% in limited heterocysts in comparison with that in vegetative cells.

© 2015 Elsevier B.V. All rights reserved.

1. Introduction

All chemical energy in the biosphere on Earth is mostly attributable to photosynthesis, the primary step of which is a conversion from a solar photon to transmembrane charge separation in chloroplasts of plants and algae or some photosynthetic prokaryotes including cyanobacteria. Although most of the absorbed photons by photosynthetic pigments are used to drive the charge separation and subsequent synthesis of energy-rich chemicals, some minor portion of photons are reemitted as autofluorescence or dissipated as heat. Autofluorescence of photosynthetic pigments, especially that of chlorophyll *a* (Chla), has been thus widely and extensively monitored as an index of photosynthetic reactions in oxygenic photosynthetic organisms [1,2]. Microscopic fluorescence images of Chla is also useful for understanding the structures and photochemical functions of thylakoid membrane in chloroplasts of plants and cyanobacterial cells under physiological conditions [3–5]. Fluorescence spectral acquisition in microscopic imaging has also been successful to obtain images of important photosynthetic molecular components like photosystem I (PSI), photosystem II (PSII), and light-harvesting molecules [4,6–12]. However, fluorescence intensity suffers from attenuation due to absorption, refraction and scattering during transmission through the samples between focus plane of interest and microscope objective. This leads to deformation of fluorescence spectra, because the attenuation of signals is dependent on fluorescence wavelength [11].

Fluorescence lifetime (FL) measurement function has been recently implemented in laser scanning confocal fluorescence microscopy in order to obtain an image with fluorescence decay parameters in all pixels (Fluorescence Lifetime Imaging Microscopy, FLIM) [4,13]. Time constants of fluorescence decay are robust parameters against

Abbreviations: APC, allophycocyanin, light-harvesting subunit of phycobilisome; CF, chlorophyll fluorescence; CFL, chlorophyll fluorescence lifetime; Chla, Chlb, chlorophyll a, chlorophyll b; CP26, CP29, light-harvesting complex of photosystem II; FL, fluorescence lifetime; FLIM, Fluorescence Lifetime Imaging Microscopy; FWHM, full width at half maximum; IRF, instrument-response function; LHCI, light-harvesting complex of photosystem I; LHCII, light-harvesting complex of photosystem II; NPQ, nonphotochemical quenching; PAM, Pulse-amplitude-modulation fluorometry; PBS, phycobilisome; PC, phycocyanin, light-harvesting subunit of phycobilisome; PEC, phycoerythrocyanin, light-harvesting subunit of phycobilisome; PSI, PSII, photosystem I, photosystem II; Q_A, electron acceptor quinone in photosystem II.

* Corresponding author at: Department of Chemistry, Graduate School of Science, Kyoto University, Kyoto 606-8502, Japan.
E-mail address: kumazaki@kuchem.kyoto-u.ac.jp (S. Kumazaki).

http://dx.doi.org/10.1016/j.bbabio.2015.10.003
0005-2728/© 2015 Elsevier B.V. All rights reserved.

attenuation, because they are just determined by the nature of distribution of the delay time between absorption of excitation photon and emission of fluorescence photon. The nature of the distribution is unchanged by the attenuation of the number of fluorescence photons, as far as attenuation is in a linear regime, under which propagation and transmission of the fluorescence does not depend on the fluorescence intensity.

Fluorescence decay on a picosecond to nanosecond time scale of thylakoid membrane reflects the time scales of energy conversion and/or dissipation from photons to chemical energy and/or heat. It is thus expected that FLIM can be used to a wide range of studies on thylakoid membrane in plants, algae and cyanobacteria. There are already a substantial number of applications of FLIM to study many aspects of thylakoid membrane in vivo by visible short pulses [14–17]. Two-photon excitation has also been tested in the application of FLIM to chloroplasts [18–21]. However, there still remain several uncertainties in the potential and limitations in the FLIM measurements. First, excitation power dependence of the FLIM data has not been sufficiently documented. There are hundreds of photosynthetic pigments that can exchange electronic excitation energy. It is thus possible that annihilations between multiple excited pigments (singlet–singlet, singlet–triplet etc.) can lead to an abnormally fast decay of fluorescence [18,22,23,24]. It is also well known that strong pulse and/or continued illumination on the same sample region can temporarily convert substantial portion of reaction centers of PSII into charge-separated state that cannot perform primary charge separation (closed PSII). The closed PSII shows a longer fluorescence lifetime (about 0.7–2 ns) than PSII that is ready for the primary charge separation (about 0.17–0.4 ns, open PSII) [15,18,21,25–29,30,31]. The effects of annihilation and the open-closed status of PSII to the actual FLIM images can be predicted only if scanning parameters of the excitation laser, absorption cross section of PSII and transition rate from closed PSII to open PSII are all properly considered. Second, contribution of PSI to the chlorohyll fluorescence (CF) at physiological temperature has not been sufficiently characterized. PSI fluorescence is most conventionally measured at cryogenic temperatures, because fluorescence quantum yield from PSI and/or its closely associated antenna like light-harvesting complex I (LHCI) in chloroplasts are relatively enhanced in comparison with that of PSII [1]. However, PSI fluorescence at physiological temperatures is not negligible [26,32,33]. The lifetime of PSI fluorescence (about 0.025–0.12 ns) is generally reported to be independent of excitation light intensity and shorter than that of PSII [26,28,34–36]. It is then likely that the image of PSII/PSI ratio in various chloroplasts/cells can be potentially obtained if dependence of fluorescence lifetimes on laser power is obtained. It is thus desirable to accumulate examples of FLIM measurements on various types of thylakoid membranes with different ratios of PSI/PSII.

Based on the above background, we have conducted FLIM measurements of an algal chloroplast and cyanobacterial cells with systematically varied excitation laser power. Our FLIM system has two channels of rigorously simultaneous fluorescence detection, largely corresponding to PSII and PSI. As a first test, we have avoided multicellular organisms in which it is difficult to estimate excitation power reaching a target focal plane. We have selected a filamentous diazotroph, *Anabaena variabilis* (*A. variabilis*), which contains differentiated cell, heterocyst. It is well known that the PSII content in matured heterocyst is far lower than that of vegetative cells in the same filament [9,10,37]. It is thus expected that FL of PSI-rich thylakoid membrane in the heterocyst can be obtained and compared with that of vegetative cells having substantial PSII in addition to PSI. As a second example, a unicellular green alga, *Parachlorella kessleri* (*P. kessleri*) was selected, because it lacks motility and has chlorophyll-based light-harvesting complexes [38,39]. Our available excitation wavelength was 404 nm, at which chlorophyll-based light-harvesting systems show far greater absorption cross section than phycobilin-based antenna, phycobilisome (PBS), of cyanobacteria. It is then likely that multiple excitation effects in the single PSI and/or PSII units are more sensitively observed in the *P. kessleri* than in *A. variabilis*. In addition, we have composed a numerical simulation that almost fully reflects all relevant parameters: absorption cross section of PSII and its associated light-harvesting complexes, decay time constants of closed PSII (recovery time constant of open PSII) and laser-scanning parameters in the actually employed FLIM conditions. The simulation can largely reproduce experimental sensitivity of the FL to the absolute laser power. As an application example of our methodology, possible indication of functional PSII in the PSI-rich heterocyst was examined in detail. There have been reports on the presence of transcripts and proteins of PSII reaction centers in isolated heterocysts [40–42]. PSII activity in heterocysts in filaments in vivo was also reported by single cell variable fluorescence intensity [5]. These observations raised a question of how oxygen-sensitive nitrogenase for the nitrogen-fixation is compatible with the function of PSII in the heterocysts. Our methodology will hopefully add one more experimental observation on this interesting issue on a single cell basis in intact filaments.

2. Experimental

A. variabilis cells (strain NIES-2095) were purchased from the microbial culture collection at the National Institute of Environmental Studies (Tsukuba, Ibaraki, Japan). The cell filaments were grown photoautotrophically in nitrogen-free BG-11 medium (removing $NaNO_3$ and replacing ferric ammonium citrate with ferric citrate in the BG-11 formulation [43]) for 3, 24, or 90 days at 29 °C under a 15-h light/9-h dark photoperiod after an inoculation. The same nitrogen-free BG-11 medium was also used before the inoculation. The photosynthetic photon flux density at the sample position in an incubator was about 20 μmol photons m^{-2} s^{-1}. A cell suspension after a suitable dilution was transferred to glass-bottom dish (D111505, Matsunami, Osaka, Japan). One piece of agar was put on the cell suspension in order to immobilize cells at the surface of the cover glass. All microspectroscopic measurements were started after 15–20 min of dark adaptation period on the microscope stage (Table S1).

P. kessleri cells were purchased from the IAM culture collection as IAM C-531 (now maintained as NIES-2160 in the microbial culture collection, at the National Institute of Environmental Studies, Tsukuba, Ibaraki, Japan). The cells used for measurement were grown photoautotrophically in 40 cm^3 of BG-11 incubation medium in the same incubator as *A. variabilis* for 15 or 29 days after an inoculation. The preparation for the microscopic observation was also the same as used for *A. variabilis* cells. All microspectroscopic measurements were started after 15–20 min of dark adaptation period on the microscope stage (Table S1).

Autofluorescence images and lifetimes of the cells were obtained by a laser-scanning confocal imaging system (DCS-120, Becker & Hickl GmbH) with time-correlated single photon counting (TCSPC) boards (SPC-152, Becker & Hickl GmbH). The glass-bottom dish containing cells was mounted on an inverted microscope (IX-71, Olympus), with which the confocal scanner (DCS-120) was coupled. Photosynthetic pigments were excited by the second harmonic beam (404 nm) of a mode-locked Ti:Sapphire oscillator (Coherent) with a repetition rate of 75.5 MHz. Two detection channels with band-path filters (673–698 nm and 703–740 nm) were simultaneously used to see mainly CF, which largely corresponds to PSII and PSI. The wavelength regions were optically selected by combinations of a long-wavelength-passing beam splitter (with an edge wavelength at 700 nm) and two band-pass filters. Residual laser light was rejected by long-wavelength-passing filter with an edge wavelength at about 500 nm. The obtained datasets of FL images were analyzed using image analysis software (SPCImage, Becker & Hickl GmbH), and some kinetic traces of selected regions were fitted by Igor Pro (version 6, e.g., Figs. S1–S5). Images at different depth positions were obtained by using a piezo actuator for changing the focus of an oil-immersion microscope objective (Olympus UPLSAPO, 100XO, NA = 1.40). The excitation intensity of the laser was

automatically controlled by a filter wheel with neutral density filters of different transmissions. A laser power of 20 nW at the sample position was confirmed by a power meter (PD-300-SH & NOVA, Ophir), and weaker laser powers were achieved by the filters of known transmission at 404 nm. Confocal pinhole sizes for the two fluorescence bands were manually changed between FLIM acquisitions at different laser powers (Table S1), by which the maximal probability of detection of fluorescence photons per single excitation pulse was limited to at most 3×10^{-3} at the brightest spot in fluorescence images. It is thus to be noted that fluorescence counts at different laser powers cannot be directly compared. (Figs. S2–S5). The instrument-response function (IRF) was 0.08 ± 0.015 ns at 689 nm and 0.10 ± 0.015 ns at 716 nm in full width at half maximum (FWHM). One test on time-resolution is shown in Fig. S1. The curve with a time constant of 0.084 ns obtained in the constraint-free fitting is clearly better than that in the constrained fitting with a fixed time constant of 0.050 ns. As far as our data analysis is based on data with a comparable s/n or better, the distinguishability of the time constant is at worst about 0.03 ns (30 ps).

3. Results

3.1. Fluorescence lifetime imaging

FLIM measurements at varied laser intensities of *A. variabilis* were performed on 22 filaments of cells (or trichomes) including a total of about 190 vegetative cells and 22 heterocysts. One set of data is shown in Fig. 1. The cells in the image panels are all vegetative cells except one heterocyst indicated by white (Figs. 1(a)–(o)) or black

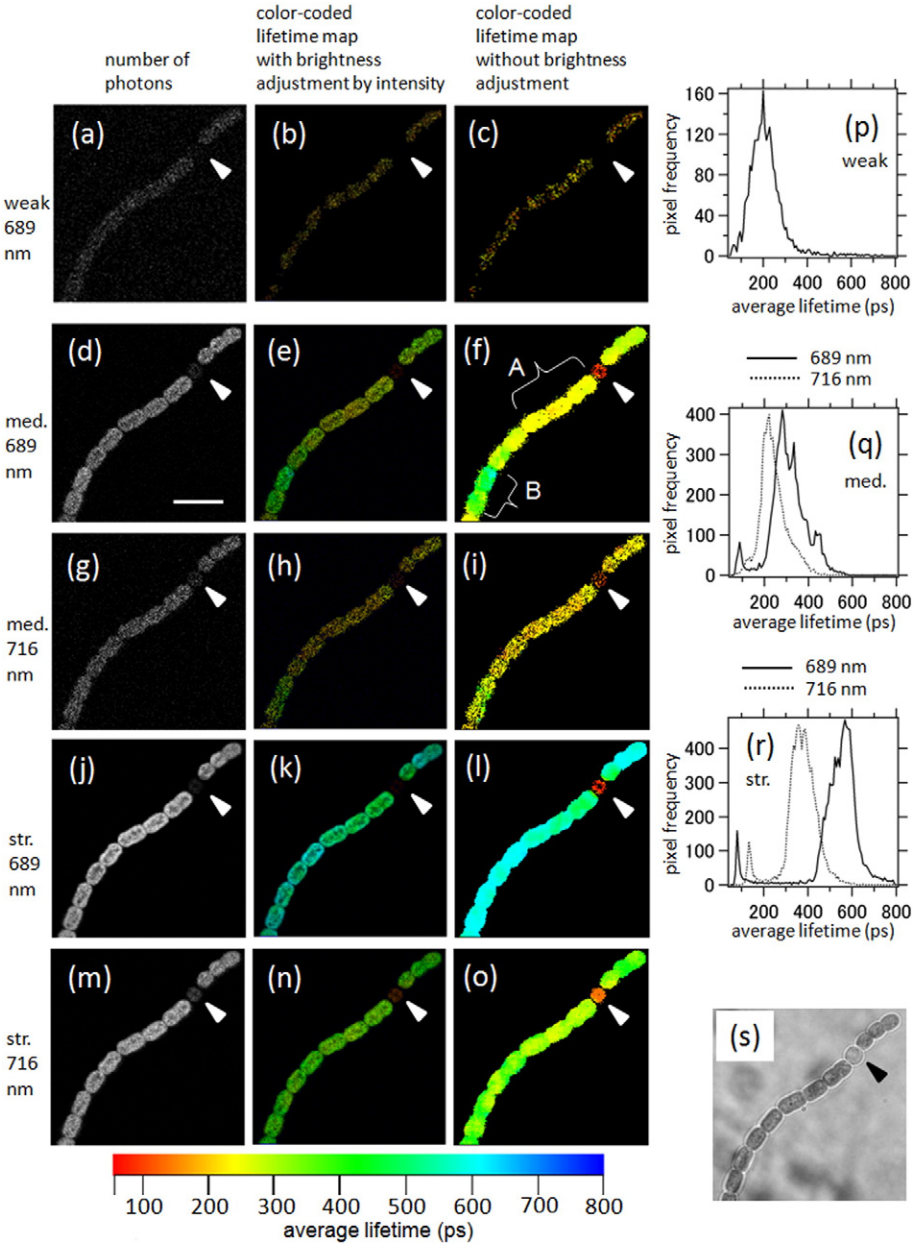

Fig. 1. Characteristics of average fluorescent lifetime images *A. variabilis* at different laser powers and detection wavelengths in the FLIM measurements. Excitation laser power at the sample position was 0.08 nW (weak), 1.1 nW (med.) and 20 nW (str.) in (a–c), (d–i) and (j–o), respectively. The laser powers and detection wavelength (centered at 689 nm or 716 nm) are shown on the left. (a), (d), (g), (j), (m): Photon count-based fluorescent images. (b), (e), (h), (k), (n): Corresponding average fluorescent lifetime images with intensity-dependent brightness adjustment. (c), (f), (i), (l), (o): Corresponding average fluorescent lifetime images without the brightness adjustment. (p), (q), (r): Distributions of average fluorescence lifetime at the three different laser intensities. (s): Bright-field image of the same area. Scale bar in (d) is equal to 10 μm and applicable to all the image panels. The effective spatial resolution in the color-coded average FL images is about 1.94 μm due to the binning of 11 × 11 pixels.

(Fig. 1(s)) arrow heads. Three levels of excitation laser power, 0.08, 1.1 and 20 nW at the sample position were employed in this order (Table S1) in one set of experiments on 6 filaments containing 6 heterocysts that were 90 days after inoculation (Tables S2,S3). Five levels of excitation laser power, 0.08, 0.30, 1.1, 5.3 and 20 nW at the sample position were also analogously employed in this order in the other two independent sets of experiments on filaments harvested 3 and 24 days after inoculation (7 and 9 filaments containing 7 and 9 heterocysts, respectively)(Tables S2, S3). In order to check damage or any long-lived actinic effects of previous laser scans on the sample, a FLIM measurement with the lowest power at 0.08 nW was always repeated after the measurement at the highest laser power (Fig. S2,S3, Table S1). Average FL at each pixel,$<\tau>$, was calculated according to the following formulae,

$$F(t) \approx \int_{-\infty}^{+\infty} IRF(s) \begin{cases} A_0 + A_1 \exp\left[-\dfrac{(t-s)}{\tau_1}\right] + A_2 \exp\left[-\dfrac{(t-s)}{\tau_2}\right] & , \quad t \geq s \\ 0 & , \quad t < s \end{cases} ds, \tag{1}$$

$$\langle \tau \rangle = (A_1\tau_1 + A_2\tau_2)/(A_1 + A_2), \quad \tau_1 < \tau_2, \tag{2}$$

where temporal profile of fluorescence intensity at the pixel, $F(t)$, was fitted by convolution of a sum of two exponential functions with the instrument-response function, $IRF(s)$, (as Eq. (1)). The fitting yielded exponential decay time constants, τ_1 and τ_2, and their amplitudes, A_1 and A_2, in addition to a non-decaying component, A_0. Our measurement time window was only between minus 0.3 ns and plus 2.7 ns, and the pulse-to-pulse interval in the excitation laser was 13.24 ns. The amplitude of A_0 thus suggests a long-lived fluorescence with an approximate lifetime between 2 and 13 ns. A_0 was always set to be zero in the SPC image analysis program. When fluorescence decay profiles were later extracted from certain specified areas of cells, amplitude of A_0 were set to be non-negative and they were typically 0–1% or at most 2–3% in a very few cases with a relatively poor s/n, which does not affect our following discussion (Tables 1–3 and S2–S4). In using the SPCimage analysis program for *A. variabilis*, a binning of pixels was performed in which photon data in 11 × 11 raw pixels (square region of about 1.94 × 1.94 μm) were all included to obtain a fluorescence decay profile at the center pixel. This binning was employed at all the laser power levels, which enabled us to obtain the color-coded images of average FL of cells even at the weakest laser power employed. However, it caused degradation of apparent spatial resolution in the average FL map. As the laser power is increased, the lifetimes in the whole filament except the heterocyst are elongated. At the weakest laser power of 0.08 nW, the most frequent average FL obtained at 689 nm is around 200 ps (Fig. 1(p)). The average FL at 689 nm given by the middle (1.1 nW) and strongest laser power (20 nW) are 300 and 570 ps, respectively (Fig. 1(q) and (r)). This elongation of average FL is evident in all the vegetative cells in both the two detection channels (689 and 716 nm). The FL of the heterocysts does not show obvious elongation. It is to be noted that contribution of the heterocyst to the lifetime histogram is recognized as a small peak around 0.08–0.09 ns and 0.12–0.13 ns in the cases of 689 nm and 716 nm, respectively (Fig. 1(q) and (r)).

Multi-exponential nature of the fluorescence decay is not visualized in the map of average FL like Fig.1. Photon counting data, which are photon counts versus arrival times, were separately collected from the vegetative cells and heterocyst, which gave fluorescence decay traces (Fig. 2(a)–(c), S2–S4). Before the curve fitting by Eq. (1), average photon counts in the sufficiently negative time region (For example, 5–10 and 3–19 counts per time channel in the 689 and 716 nm wavelength channels, respectively, for the traces shown in Fig. S2) was subtracted. It is thus possible that artificially negative photon counts arise (Figs. 2, S2–S5). These counts at negative times remained in the above-mentioned range even when the laser power was increased by 200 times. It is thus unlikely that the subtracted counts are attributable to short-lived laser-induced transient phenomena in samples (<10 s). These small signals are thus not considered in this work. All types of fluorescence traces in the two cellular types (heterocysts or vegetative cells), with the two center wavelengths of detection (689 or 716 nm), and with the three or five different laser intensities were fitted by the sum of two decaying exponential components (Eq. (1), Tables 1, 2, Figs. 2, S2–S4). When the two exponential time constants are not separated well due to intrinsic nature of the decay and/or signal-to-noise, single decaying exponential function was used. The judgment was also supported by the reduced chi square values (Figs. S2–S4). Although some reduced chi square values are substantially larger than 1, we focus

Table 1
Parameters yielded by curve fitting of the FLIM data of vegetative cells of *A. variabilis*.

λ_{fl} [nm]	P_{laser} [nW]	τ_1[ns] (Amplitude in %)	τ_2 [ns] (Amplitude in %)	∞ (Amplitude in %)	Average lifetime [ns]
689[a]	0.08	0.22[a] ± 0.01[c] (97.5[a](+2.5 / −1.5)[c])	1.09[a](±0.00 / −0.34)[c] (2.5[a] ± 2.5)[c]	(0.0[a](+1.5/−0.0)[c])	0.25[a](+0.00 / −0.03)[c]
	0.30	0.23(+0.00 / −0.01) (96)	0.88(+0.00 / −0.09) (4)	(0)	0.25
	1.1	0.23(+0.01 / −0.02) (85(+3 / −5))	0.74(+0.03 / −0.12) (15(+5 / −3))	(0)	0.31(+0.03 / −0.04)
	5.3	0.26(+0.00 / −0.02) (67(+5 / −10))	0.80(+0.00 / −0.08) (33(+10 / −5))	(0)	0.43 ± 0.05
	20	0.25 ± 0.02 (62(+8 / −9))	0.75 ± 0.05 (37(+10 / −7))	(0.5 ± 0.5)	0.44(+0.03 / −0.05)
716[b]	0.08	0.225[b] ± 0.005[c] (99.5[b] ± 0.5[c])	n.d.	(0[b])	0.225[b] ± 0.005[c]
	0.30	0.225 ± 0.005 (100)	n.d.	(0)	0.225 ± 0.005
	1.1	0.23 ± 0.01 (95.5 ± 2.5)	1.13 ± 0.18 (4.5 ± 2.5)	(0)	0.25
	5.3	0.23 (85 ± 3)	0.88 ± 0.05 (15 ± 3)	(0)	0.33 ± 0.03
	20	0.225 ± 0.015 (84 ± 3)	0.85 ± 0.05 (16 ± 3)	(0)	0.34

[a] These parameters in the case of fluorescence at 689 nm were given by the curve fitting of the sum of all available data (3 independent experiments) at the same laser excitation power to the double exponential function convoluted with the IRF. See Table S2 for the parameters separately obtained for the three sets of experiments.
[b] These parameters in the case of fluorescence at 716 nm are given as the average values obtained by the curve fitting for the two or three independent experiments (See Table S2).
[c] All error bars in this table are given so as to cover the differences between the multiple data sets that were acquired independently (See Table S2).

Table 2
Parameters yielded by curve fitting of the FLIM data of heterocysts of *A. variabilis*.

λ_{fl} [nm]	P_{laser} [nW]	τ_1[ns] (Amplitude in %)	τ_1[ns] of the subsets[c] (Amplitude in %) upper :w/o lower:w/	τ_2 [ns] (Amplitude in %)	τ_2[ns] of the subsets[c] (Amplitude in %) upper :w/o lower:w/	∞ (Amplitude in %)	Average lifetime [ns]	Average lifetime of the subsets[c] upper :w/o lower:w/ [ns]
689[a]	0.08	0.087[a] ± 0.009[b]	0.084(99)	n.d.	n.d.		0.087	0.084
		(99[a] ± 1[b])	0.072(91)		0.57(8)	(1[a] ± 1[b])		0.112
	0.30	0.089 ± 0.005	0.084	n.d.	n.d.		0.089	0.084
		(99.5 ± 0.5)	(100)			(0.5 ± 0.5)		
			0.088(88)		0.69(11)			0.155
	1.1	0.080 ± 0.002	0.078(98)	0.86 ± 0.25	0.64(2)		0.112	0.089
		(96 ± 2)	0.092(89)	(4 ± 2)	0.74(10)	(0)		0.157
	5.3	0.081 ± 0.002	0.075(98)	0.855 ± 0.25	0.67(2)		0.108	0.087
		(96.5 ± 1.5)	0.088(87)	(3.5 ± 1.5)	0.70(12)	(0)		0.162
	20	0.081 ± 0.003	0.075(98)	1.03 ± 0. 39	0.70(2)		0.129	0.088
		(94.5 ± 3.5)	0.085(88)	(5 ± 3)	0.70(11)	(0.5 ± 0.5)		0.153
716[a]	0.30	0.145 ± 0.005	n.a.	n.d.	n.a.			
		(100)				(0)		
	1.1	0.14 ± 0.01	n.a.	n.d.	n.a.			
		(100)				(0)		
	5.3	0.14	n.a.	n.d.	n.a.			
		(100)				(0)		
	20	0.14 ± 0.01	n.a.	n.d.	n.a			
		(100)				(0)		

[a] These parameters in the two wavelength regions are given as the average values between maximum and minimum obtained by the curve fitting for the three independent experiments (See Table S3).
[b] All error bars in this table are given so as to cover the differences between the multiple data sets that were acquired independently (See Table S3).
[c] One of the subsets of heterocysts (subset/w) includes 5 heterocysts with a substantial amplitude of long-lived fluorescence (>0.6 ns). The other subset of heterocysts (subset/w/o) includes 17 heterocysts with a relatively small amplitude of long-lived fluorescence (>0.6 ns).

on the approximate description of the whole data by at most two exponential functions, which is mainly for the consistency with the simulation framework (See Sections 3.2 and 4.6). It is to be noted that the short lifetime component of vegetative cell is limited in a very narrow range (0.22–0.26 ns in Table 1), which seems to be independent of the center wavelength of the fluorescence detection and the excitation laser powers employed, even though we did not impose any linkage of parameters (so-called globally common parameters) in the curve fitting between the different fluorescence traces. This lifetime is in good agreement with the most dominant component observed in an ensemble of cells of *A. variabilis* (0.22 ns and 85%) [44]. It is also largely comparable to CFL observed in other cyanobacteria at room temperatures (Table S6) [34,36,45–47]. The average FL of the vegetative cell gradually increases as the excitation power is raised, which is caused by the increase of the long lifetime component with time constants of 0.74–1.09 ns and 0.85–1.13 ns at the detection wavelengths of 689 and 716 nm, respectively (Fig. 2(a), Table 1, Fig. S2). These behaviors are largely consistent with those reported in another cyanobacterium *Synechococcus* 6301 by raising the level of closed PSII [46].

In the sum of FLIM data of all 22 heterocysts, at least 94% of its fluorescence decays with a time constant of 0.080–0.089 ns and 0.14 ns at 689 and 716 nm, respectively, at all the excitation powers (Table 2, Fig. S2). There is a minor long-lived component with a time constant of 0.86–1.03 ns. Since single-cell fluorescence spectra and photochemical behavior changes during differentiation process [5,9,10,48,49], it is likely that FLIM data from randomly selected heterocyst are

Table 3
Parameters yielded by curve fitting of FLIM data of *P. kessleri*.

λ_{fl} [nm]	P_{laser} [pW]	τ_1[ns] (Amplitude in %)	τ_2 [ns] (Amplitude in %)	∞ (Amplitude in %)	Average lifetime [ns]
689[a]	4	0.32[a](+0.08 / −0.04)[c]	0.82[a](+0.00 / −0.20)[c]		0.38[a] (+0.02 / −0.02)[c]
		(88 (+11 / −5)[c])	(12(+5 / −12)[c])	(0(+1 / −0)[c])	
	15	0.28	0.63		0.36
		(77)	(23)	(0)	
	55	0.29(+0.00 / −0.00)	0.70(+0.00 / −0.02)		0.39 (+0.03 / −0.01)
		(75(+1 / −9))	(25(+9 / −1))	(0)	
	265	0.29	0.83		0.50
		(61)	(39)	(0)	
	1.0	0.33 ± 0.01	1.24 ± 0.06		0.81 (±0.04)
	×10^3	(47 ± 1)	(53 ± 1)	(0)	
716[b]	15	0.32[b] (95)	0.87[b](5)	(0)	0.34[b]
	55	0.37 ± 0.03	n.d.		0.37
		(100)		(0)	
	265	0.36 (90)	1.3(10)	(0)	0.45
	1.0–1.2	0.365 ± 0.005	1. 4 ± 0.1		0.655 ± 0.025
	×10^3	(72)	(28)	(0)	

[a] These parameters in the case of fluorescence at 689 nm were given by the curve fitting of the sum of all available data (2 independent experiments) at the same laser excitation power to the double exponential function convoluted with the IRF. See Table S4 for the parameters separately obtained for the two experiments.
[b] These parameters in the case of fluorescence at 716 nm are given as the average values obtained by the curve fitting for the two independent experiments (See Table S4).
[c] These error bars are given so as to cover the ranges of the parameters separately obtained for the multiple data sets that were acquired independently (See Table S4).

heterogeneous, which may reflect developmental stage or age of each heterocyst. The 22 heterocysts that we analyzed were classified into two subsets (17 and 5 heterocysts) based on an approximate single-exponential curve fittings of the 689 nm fluorescence kinetics of individual heterocysts at the highest laser power (20 nW). The lifetimes of 689 nm fluorescence kinetics of the first subset (17 heterocysts) are shorter than those of the second one (5 heterocysts). The former and the latter subsets are designated as subset/w/o (without a substantial long-lived component) and subset/w/ (with a substantial long-lived component). Sum of photon data were separately prepared from the two subsets (Fig. 2(b) and (c), Table 2, Fig. S4). The subset/w/ has a long-lived component even at the weakest laser power (0.57 ns, 8%) that was distinguishable from infinitely long-lived component (with an approximate time constant of 2–13 ns) and the amplitude of the long-lived component was constantly greater than those of the subset/w/o at all power levels (Table 2).

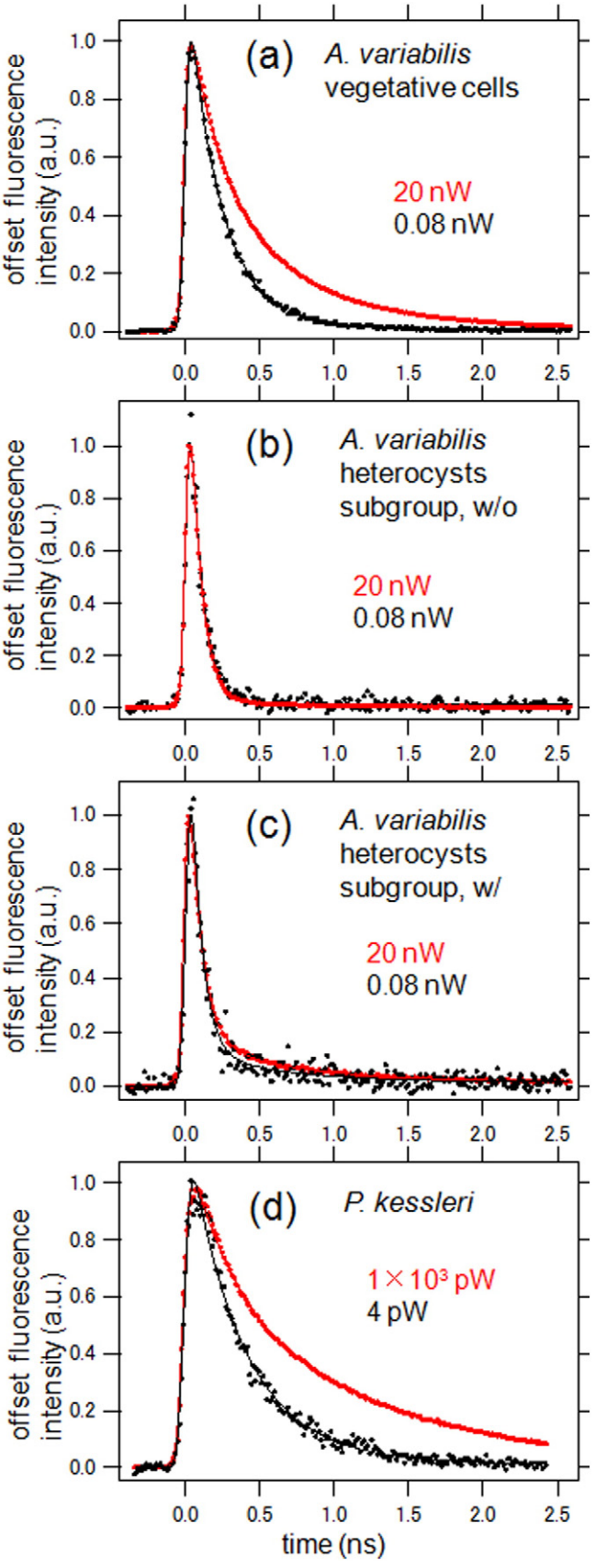

Fig. 2. Effects of incident excitation laser power on decay profiles of fluorescence centered at 689 nm. Dots represent normalized fluorescence intensities based on photon count data from which average photon counts in the sufficiently negative time region was subtracted. It is thus possible that artificially negative fluorescence intensities arise. (a) Photon count data from all vegetative cells in 22 filaments (about 8–13 cells per filament) of *A. variabilis* at single focal planes were used. (b) Selected 17 heterocysts of *A. variabilis* at two or three focal planes were used. These heterocysts were selected as having relatively low level of long-lived fluorescence at the highest laser power (See Table 2). (c) Selected 5 heterocysts of *A. variabilis* at two or three focal planes were used. These heterocysts were selected as having relatively high level of long-lived fluorescence at the highest laser power (See Table 2). (d) Photon count data from 32 cells of *P. kessleri* at 1–3 focal planes were used. Solid lines represent fitting curves made by convolution of the instrument-response function with a sum of one or two exponential functions. The parameters obtained through the curve fitting are shown in Tables 1–3. The plots in black and red represent data and fitting curves in the cases of weakest and strongest laser power levels, respectively. More examples of fluorescence decay profiles of fluorescence at both 689 and 716 nm at all employed laser power levels are shown in Figs. S2-S5.

Excitation power dependence of FLIM in the case of *P. kessleri* were obtained for 32 cells at excitation laser powers that were about one order of magnitude weaker than those of *A. variabilis* (Figs. 2(d), 3, S5, Table 3). Example of one data set, in which three cells were imaged at the same time, is shown in Fig. 3. The color-coded average FL image for the *P. kessleri* cells was obtained with a binning of 21 × 21 raw pixels (square region of about 3.7 × 3.7 μm). Three or five levels of excitation laser power, (4, 55 and 1.0×10^3 pW or 4, 15, 55, 265 and 1.0×10^3 pW) at the sample position were employed in this order (Table S1). In order to check damage or any long-lived actinic effects of previous laser scans on the sample, FLIM measurement with the lowest power at 4 pW was repeated after the measurement at the highest laser power (Fig. S5), which have shown essentially the same results as the first ones with the same power. One of the three cells (cell no. 2 in Fig. 3(m)) showed clearly longer average FL than the other two cells (cell no. 1 and 3 in Fig. 3(m)). Such a cell with exceptional lifetime was not included as the target cells of fine analysis on the fluorescence decay profiles. An elongation of the average FL was evident especially between 55 and 265 pW (Tables 3 and S4). The shortest lifetime observed in the case of *P. kessleri* was about 0.28–0.33 ns at 689 nm, which was always longer than that of the vegetative cells of *A. variabilis* (0.22–0.26 ns) (Figs. 1, 2, and Table 1).

3.2. Simulation on open-closed state of PSII under the FLIM imaging conditions

Although it seems to be well established that open and closed PSII show relatively short (0.1–0.4 ns) and long fluorescence lifetimes (0.8–2 ns), [15,21,25,28,29,26,27,31,30] (See also Tables S5 and S6 for more references), how the components appear in fluorescence kinetics under actual FLIM experimental conditions has remained unexplained in a sufficiently quantitative manner. The purpose of the computer simulation described here is to quantitatively support our hypothesis that double exponential decay observed in our FLIM measurements in vegetative cells of *A. variabilis* and *P. kessleri* (Tables 1, 3, S2, S4) is a result of

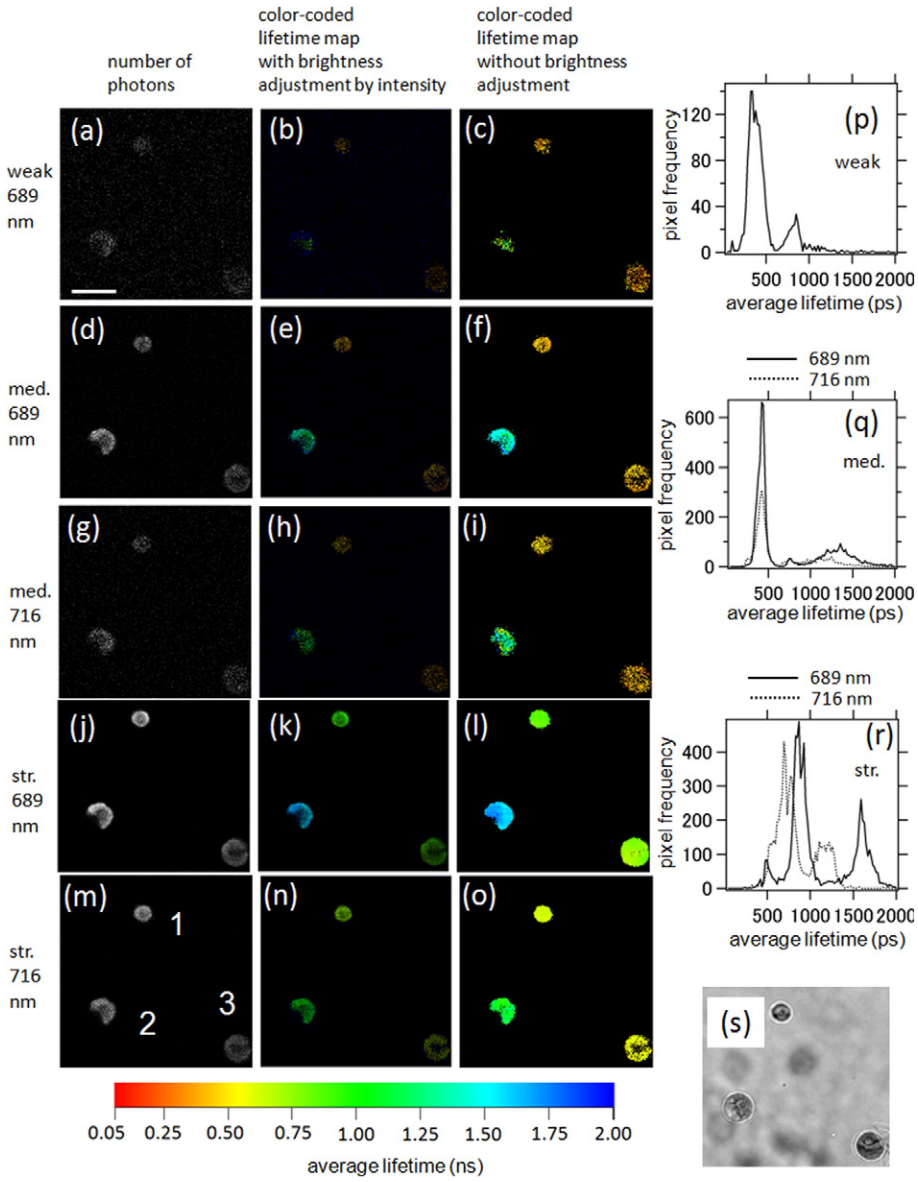

Fig. 3. Characteristics of average fluorescent lifetime images *P. kessleri* at different laser powers and detection wavelengths in the FLIM measurements. Excitation laser power at the sample position was 4 pW (weak), 55 pW (med.) and 1×10^3 pW (str.) in (a–c), (d–i) and (j–o), respectively. The laser powers and detection wavelength (centered at 689 nm or 716 nm) are shown on the left. (a), (d), (g), (j), (m): Photon count-based fluorescent images. (b), (e), (h), (k), (n): Corresponding average fluorescent lifetime images with intensity-dependent brightness. (c), (f), (i), (l), (o): Corresponding average fluorescent lifetime images without the adjustment of brightness. (p), (q), (r): Distributions of average fluorescence lifetime. (s): Bright-field image of the same area. Scale bar in (a) is equal to 10 μm and applicable to all the image panels. The effective spatial resolution in the color-coded average FL images is about 3.7 μm due to the binning of 21 × 21 pixels.

observing fluorescence from both open and closed PSII. Only an outline of the simulation is presented below and the details are fully described in Text S1.

The experimentally obtained fluorescence decay is made of fluorescence from many PSII units in the cells, but this situation is equivalently expressed by a single representative PSII unit at the position (x,y,z) = (0,0,0) with full description on the probability of open/closed status (Fig. S6 and Text S1). In the simulation, a laser beam focus is moved in a manner of raster scan around the PSII, as in the experiments. Excitation probability of the PSII unit by a single laser pulse is assumed to be given by the single pulse laser energy, a Gaussian laser intensity profile, position of the laser focus, and an effective absorption cross section of PSII at the laser wavelength (404 nm) (Fig. S6 and Text S1). Once the PSII in the open state is optically excited, it is converted into a closed PSII with a probability of the photosynthetic charge separation. The time-dependent populations of open PSII and closed PSII in a unit volume, $N_{\mathrm{open}}(t_{\mathrm{m}})$ and $N_{\mathrm{closed}}(t_{\mathrm{m}})$, or their proportional quantities that are probabilities for the PSII to be open or closed, $p_{\mathrm{open}}(\mathrm{t})$ or $p_{\mathrm{closed}}(\mathrm{t})$, are calculated as follows (Text S1).

$$\begin{aligned}\begin{bmatrix} N_{\mathrm{open}}(t_{m+1}) \\ N_{\mathrm{closed}}(t_{m+1}) \end{bmatrix} &= \begin{bmatrix} N_{\mathrm{PSII}} p_{\mathrm{open}}(t_{m+1}) \\ N_{\mathrm{PSII}} p_{\mathrm{closed}}(t_{m+1}) \end{bmatrix} = N_{\mathrm{PSII}} \begin{bmatrix} p_{\mathrm{open}}(t_{m+1}) \\ 1-p_{\mathrm{open}}(t_{m+1}) \end{bmatrix} \\ &= N_{\mathrm{PSII}} \begin{bmatrix} 1-0.80 p_f\left(j_y(t_m), j_x(t_m)\right) & \{1-\exp[-(t_{m+1}-t_m)/\tau_{\mathrm{R}}]\} \\ 0.80 p_f\left(j_y(t_m), j_x(t_m)\right) & \exp[-(t_{m+1}-t_m)/\tau_{\mathrm{R}}] \end{bmatrix} \\ &\quad \begin{bmatrix} p_{\mathrm{open}}(t_m) \\ 1-p_{\mathrm{open}}(t_m) \end{bmatrix}, \end{aligned} \tag{3}$$

where t_{m} and $t_{\mathrm{m}+1}$ represent a time in the simulation and its subsequent time, respectively, N_{PSII} the total population of PSII in a unit volume (assumed to be constant), $p_{\mathrm{f}}(j_{\mathrm{y}}(t_{\mathrm{m}})$ and $j_{\mathrm{x}}(t_{\mathrm{m}}))$ the probability

for the PSII to be excited by the laser pulses between t_m and t_{m+1}, $j_y(t_m)$ and $j_x(t_m)$ are x (horizontal-axis) and y (vertical-axis) interger coordinates with a unit length of 25 nm of the laser beam at the time t_m, respectively, τ_R the time constant for the closed PSII to be converted back into open state. The excitation probability function, p_f in Eq. (3) (and in Eqs. (4)–(5) (*vide infra*)), is set to be two-dimensional Gaussian and non-zero only when $-10 \le j_y(t_m) \le +10$ and $-10 \le j_x(t_m) \le +10$. This means that PSII is excited only when the laser spot resides in the square of a side length of 500 nm that is centered at PSII (See Supplemental Fig. S6 and Text S1). Closed PSII is set to be generated from the optically excited PSII supercomplex with a probability of 0.80, which is the most typical parameter F_v/F_m of dark-adapted chloroplasts in the pulse-amplitude-modulation fluorometry (PAM) [50–52]. The same yield was also applied to the case of *A. variabilis*, because similar F_v/F_m values are obtained in phycobilisome-lacking and/or PSII-enriched cyanobacterial mutants [53,54]. The numbers of fluorescence photons from open and closed PSII units are proportional to the populations of open PSII and closed PSII before each excitation, respectively. Thus, the experimentally obtained ratios of short-lived and long-lived fluorescence components were compared with the following time-integrated sum of the product between excitation probability and populations of open and closed PSII units at each simulation time, respectively.

$$\begin{aligned} F_{\mathrm{open,accum}} &\propto \sum_{s=1}^{2\mathrm{or}3}\sum_{k=1}^{29}\sum_{i=N_{y1}}^{N_{y2}}\sum_{j=-N_x}^{+N_x} p_f\left(7i+\left\{{}^{\Delta_{\mathrm{offset}}}/_{25}\right\},j\right)N_{\mathrm{PSII}}p_{\mathrm{open}}\left(t_{j,i,k,s}\right) \\ &= N_{\mathrm{PSII}}\sum_{s=1}^{2\mathrm{or}3}\sum_{k=1}^{29}\sum_{i=N_{y1}}^{N_{y2}}\sum_{j=-N_x}^{+N_x} p_f\left(7i+\left\{{}^{\Delta_{\mathrm{offset}}}/_{25}\right\},j\right)p_{\mathrm{open}}\left(t_{j,i,k,s}\right) \end{aligned} \tag{4}$$

$$\begin{aligned} F_{\mathrm{closed,accum}} &\propto \sum_{s=1}^{2\mathrm{or}3}\sum_{k=1}^{29}\sum_{i=N_{y1}}^{N_{y2}}\sum_{j=-N_x}^{+N_x} p_f\left(7i+\left\{{}^{\Delta_{\mathrm{offset}}}/_{25}\right\},j\right)N_{\mathrm{PSII}}\left\{1-p_{\mathrm{open}}\left(t_{j,i,k,s}\right)\right\} \\ &= N_{\mathrm{PSII}}\sum_{s=1}^{2\mathrm{or}3}\sum_{k=1}^{29}\sum_{i=N_{y1}}^{N_{y2}}\sum_{j=-N_x}^{+N_x} p_f\left(7i+\left\{{}^{\Delta_{\mathrm{offset}}}/_{25}\right\},j\right)\left\{1-p_{\mathrm{open}}\left(t_{j,i,k,s}\right)\right\} \end{aligned} \tag{5}$$

where the previously used index m and time t_m in Eq. (3) is replaced with a new set of indices j, i, k, s that reflect actual raster scan of the laser. The index j corresponds to different horizontal positions of the laser focus at a constant vertical position, i to different vertical positions of the laser focus in a single focal plane, k to different frames for accumulation in the same focal plane, and s to different focal planes. The integer coordinates, $7i + (\Delta_{\mathrm{offset}}/25)$ and j corresponding to j_y and j_x in the previous notations (Eq. (3)) indicate the relative location of the laser focus with respect to the position of PSII (at the origin). The parameter Δ_{offset} (varied between 0 and 175 nm with a step size of 25 nm for averaging) represents a relative vertical offset in nm between the origin (location of PSII) and one of the horizontal lines that are fastest scan axes of the laser. The actual ranges of j, i, k and s ($-N_x \le j \le +N_x$, $N_x = 10$, $N_{y1} \le j \le N_{y2}$, $N_{y2} - N_{y2} = 1$ or 2) are given by the finite size of the laser spot (with a diffraction-limited size of 176 nm for the excitation wavelength of 404 nm) and the other actual scanning parameters (See Text S1 for more details). When PSII is located in the exact focal plane, laser focus in the simulation is set to move by 25 nm along the x axis by the single step in the index j ($j \to j + 1$). The single step in the index i ($i \to i + 1$) is set to move the laser focus by 176 nm, which gives the rounded integer 7 in the Eqs. (4) and (5) (176 / 25 = 7). One should take into account the weights (w_1, w_2, w_3) of the three different time constants, $\tau_{R,1}$, $\tau_{R,2}$, $\tau_{R,3}$, for the recovery of open PSII from closed PSII [55,56]. The experimentally obtained dependence of FLIM on the laser power should be compared with a weighted average as follows (cf. Fig. S8).

$$\begin{aligned} \left\langle F_{\mathrm{open,accum}}(P_{\mathrm{laser}})\right\rangle &= \sum_{i=1}^{3} w_i F_{\mathrm{open,accum}}\left(P_{\mathrm{laser}},\tau_{R,i}\right) \\ \left\langle F_{\mathrm{closed,accum}}(P_{\mathrm{laser}})\right\rangle &= \sum_{i=1}^{3} w_i F_{\mathrm{closed,accum}}\left(P_{\mathrm{laser}},\tau_{R,i}\right) \end{aligned} \tag{6}$$

More details of this simulation is fully described in Text S1.

Relatively long-lived components (>0.6 ns) show greater weights at 689 nm than at 716 nm (Tables 1–3), which is understandable because PSII and PSI show maximum CF intensity near 689 and 716 nm, respectively [8,9,7,11,32,26] and because the FL of only PSII shows an elongation due to increase of the laser power [26,27]. It is thus reasonable that our simulation on PSII is compared with the amplitude ratio of the long-lived components at 0 ps ($A_2/(A_0 + A_1 + A_2)$ in Eq. (2)) in the 689 nm CF kinetics (Fig. 4). Contribution of PSI CF is not considered from the beginning in the simulation, but it will be later considered if its contribution is unavoidable, especially in the case of a cyanobacterium *A. variabilis* that is generally more rich in PSI than in green algae (including *P. kessleri*) [57].

One essential parameter in the simulation is the absorption cross section of PSII supercomplex, to which the excitation probability function, p_f in Eqs. (3)–(5), is proportional. The pigments of PS II monomer of *A. variabilis* was assumed to be the same as those in the core of the PSII complex from *Thermosynechococcus vulcanus* [58], in which 35 molecules of Chla, 2 molecules of pheophytin *a* and 11 molecules of β-carotene are contained. Absorption coefficients of these molecules at 404 nm (6.11×10^5 cm^{-1} mol^{-1} dm^3, 1.07×10^6 cm^{-1} mol^{-1} dm^3, and 5.59×10^5 cm^{-1} mol^{-1} dm^3 for Chla, pheophytin *a* and β-carotene, respectively) were obtained with the help of absorption spectra in several references [59–61]. When only the pigments in the monomer units are considered, the total absorption coefficient of PSII monomer at 404 nm thus amounts to 2.97×10^6 cm^{-1} mol^{-1} dm^3 (Text S2, Table S7). Cyanobacterial PSII is assumed to be in the state 2 since we have given a dark period of 15–20 min before each set of measurements (Table S1) [62,63,64]. One simulation was thus carried out with a minimal light-harvesting ability for PSII, where there is no PBS transferring energy to PSII. The reopening time constants of PSII in *A. variabilis* (the transition from closed state to open state) were assumed to be the same as those in another cyanobacterium, *Synechocystis* sp. PCC 6803 [55], in which there are three time constants (0.22 ms (68%), 2.9 ms (23%) and 13 s (9%)). The simulation yielded ratios of the accumulated number of excitations of closed PSII to the total accumulated number of excitations of PSII in *A. variabilis* at varied excitation laser power (PSII alone, dashed line in Fig. 4(a)). The possible association of PBS to PSII makes the effective absorption coefficient of PSII even larger, although the energy transfer efficiency from phycocyanin in PBS to PSII was reported to be 78% in a red alga *Porphyridium cruentum* and 86% in a cyanobacterium *Anacystis nidulans*, which was found to be substantially lower than about 100% in the transfer from Chlb to Chla in a green alga *Chlorella pyrenoidosa* [65]. The energy transfer from PBS to PSII lifts the simulation curve to the upper side, which results in an even greater gap between experimental and simulation plots (PSII + full PBS, solid line in Fig. 4(a)). On the other hand, the deviation of the simulation from experimental data can be alleviated if one considers contribution of PSI. Contribution of PBS fluorescence is not considered here, because the excitation wavelength at 404 nm was relatively preferential for Chla and the cyanobacterium was set to be state II (See also Section 4.3 and Table S7). In the modified simulation to better reproduce the experimental plot, the CF from PSI is assumed to contribute to 33% of the total amplitude at the weak excitation limit, and its lifetime (about 0.025–0.12 ns) [26,28,34–36] are safely in the short lifetime range (<0.25 ns) at all excitation laser power levels (PSII alone × (2/3), dashed and dotted line in Fig. 4(a), cf. Table 1).

In the case of *P. kessleri*, a green alga, the initial state of the thylakoid membrane before each set of FLIM measurements is state 1, because the dark period of 15–20 min was also given (Table S1) [66]. The organization of PS II supercomplex of *P. kessleri* was assumed to be the same as that proposed in the case of *Chlamydomonas reinhardtii* [67]. When light-harvesting ability per PSII is largest (state 1), there are three trimers of LHCII, one CP26 and one CP29 per PSII monomer in the model PSII complex (Text S2). The total number of pigments per monomer PSII were largely based on a reference [68]. In addition to the above-mentioned absorption coefficients for the pigments common to cyanobacterial PSII, absorption coefficients of the other pigments at 404 nm (1.45×10^5 cm^{-1} mol^{-1} dm^3, 4.75×10^5 cm^{-1} mol^{-1} dm^3, 6.01×10^5 cm^{-1} mol^{-1} dm^3, and 5.69×10^5 cm^{-1} mol^{-1} dm^3 for Chl *b*, neoxanthin, violaxanthin, lutein) were obtained with the help of several references reporting their absorption spectra and absorption coefficients at representative peaks (Table S8) [59,60,69–71]. Given the sum of all pigments per PSII monomer (124.5 Chla, 62.5 Chlb, 10 neoxanthin, 6.3 violaxanthin, 24.7 lutein, 11 β-carotene, 2 pheophytin molecules), the total absorption coefficient amounts to 1.16×10^7 cm^{-1} mol^{-1} dm^3, which yields a simulation curve designated as the equivalent number of Chla of 190 (Fig. 4(b)). We also added another simulation curve in the case where effective absorption cross section is twice (380 Chla) [72]. The decay of the closed state of PSII in *P. kessleri*, (reopening of PSII) was assumed to be the same as that in *C. reinhardtii*, in which there are three time constants (0.23 ms (73%), 46 ms (16%) and 7.5 s (11%)) [56]. We also performed an extra FLIM experiments with an excessively strong excitation power, which yielded a decay profile to be fitted by a sum of two exponential functions with time constants of 0.60 ns (33%) and 1.42 ns (67%) (Fig. S6), although the target cells measured for the Fig. S6 on a longer time scale were different from those analyzed as in Tables 3 and S4. This result is also added to the Fig. 4(b and c). The relatively short time constant of 0.60 ns at 6 nW excitation is clearly longer than those at the lower excitation powers (Tables 3 and S4). Possible presence of more than two decay time constants in the CF decay suggests that the open-closed PSII model (two-state model) is not sufficient. Given the current simulation framework and the signal-to-noise ratio, not the amplitude ratio of relatively long-lifetime component, but the average lifetime (Eq. (2)) is tentatively fitted by the simulation results as a compromise (Fig. 4(c)). The average FL at the weak limit and longest FL observed as a slowly-decaying component was averaged with weights of open and closed PSII that

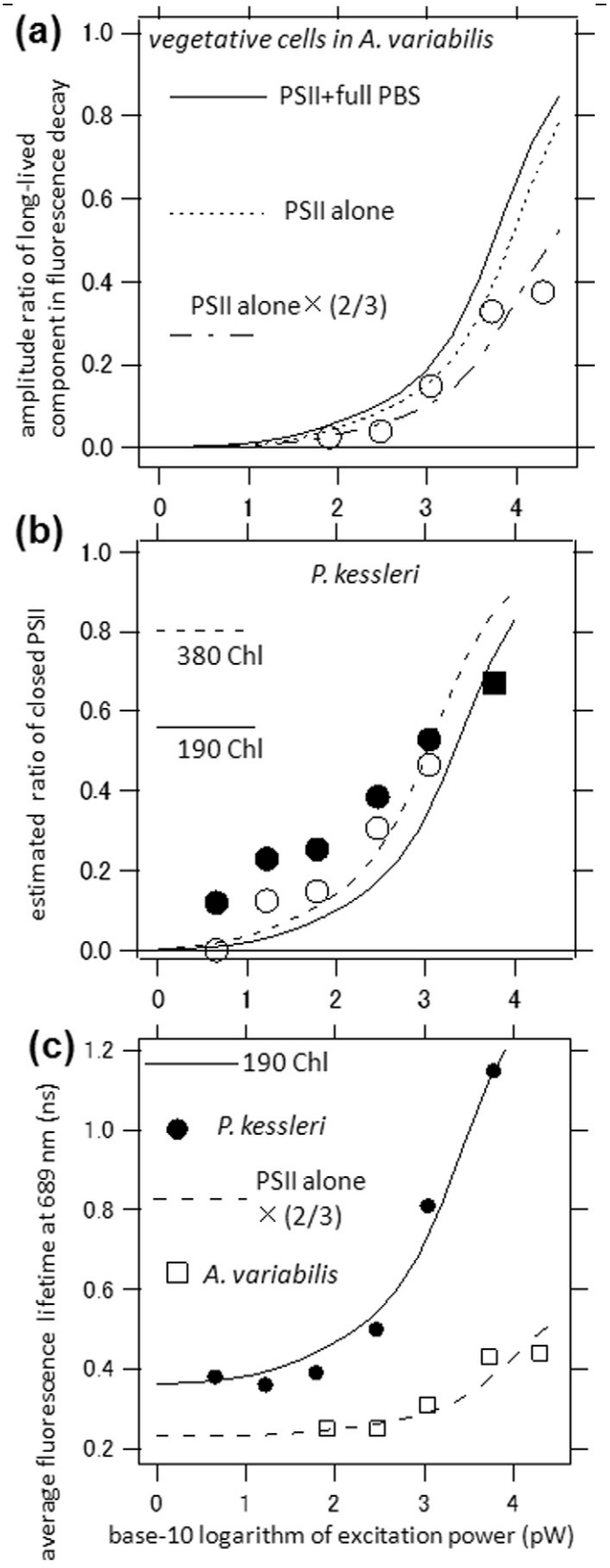

Fig. 4. Comparison between simulation and experimental parameters derived from fluorescence at 689 nm. (a) Amplitude ratios of long-lived fluorescence (>0.6 ns) at 689 nm for vegetative cells of *A. variabilis* (open circles (○), cf. Table 1). Simulated probabilities of detecting fluorescence from its closed PSII in the cases of PSII with fully extended PBS (solid line, PSII + full PBS), PSII without extra antenna (broken line, PSII alone). The dashed and dotted line (— - — - —, PSII alone × (2/3)) represent a modified plot that is a simple multiplication of the broken line (— — — —) by a factor of 0.666. This means a situation where PSI and/or PBS fluorescence is always contributing to one third of the total fluorescence at t = 0 ps and its fluorescence lifetime is always included in the relatively short lifetime (≤0.25 ns). (b) Amplitude ratios of long-lived fluorescence (>0.6 ns) at 689 nm for *P. kessleri* (closed circles (●), cf. Table 3). The data point at 6 nW ($\log_{10}(6000)$ ~3.78, closed square (■)) was obtained from a separate measurement on different cells described in Supplemental Fig. S7(e). Modified estimation of ratio of closed PSII (○), which are made from the corresponding closed circles at the same excitation power by postulating that there is a relatively long-lived component with a lifetime of 0.60–0.83 ns intrinsically from open PSII with a ratio of 12% in amplitude relative to that of the short-lived component (cf. Table 3). Solid and broken lines are ratios of closed PSII simulated in the cases of PSII having light-harvesting abilities equivalent to 190 and 380 Chla molecules, respectively. (c) Dependence of average lifetime on laser power in the vegetative cells of *A. variabilis* and *P. kessleri* cells. The solid line is given by a formula $0.36 \times (1 - R_{closed}) + 1.42 \times R_{closed}$, which is an average fluorescence lifetime in ns given by the weighted sum of those from open and closed PSII in the case of *P. kessleri*. The ratio of closed PSII, R_{closed}, is the same as the simulated curve of solid line in (b). The broken line is given by a formula $0.23 \times (1 - R_{closed}) + 0.79 \times R_{closed}$, which is an average fluorescence lifetime in ns given by the weighted sum of those from open and closed PSII in the case of vegetative cells of *A. variabilis*. The ratio of closed PSII in the total fluorescence signal, R_{closed}, is the same as the simulated curve (dashed and dotted line (— - — - —)) in (a).

were given by the simulations at varied laser intensities, which nicely reproduces the experimental average FLs.

4. Discussion

4.1. Contribution of PSI fluorescence

Chlorophyll FL (CFL) of PSI (about 0.025–0.12 ns in the previous works) in live cells have been reported by careful decomposition/deconvolution in wild type cells [26,31,35] or from PSII-deficient mutant cells that were grown heterotrophically [34,36,73]. To the best of our knowledge, the CF obtained from single heterocysts of *A. variabilis* in this work is probably a rare example in that CF in wild-type intact cells is almost purely attributable to PSI. However, it should be noted that PSI in heterocyst may be associated with the so-called rod part of PBS (consisting of phycocyanin (PC) and phycoerythrocyanin (PEC)) [9,41,74–76]. The high purity of the PSI (nearly negligible contribution by PSII) in the heterocysts is supported by several features, although possible minor contribution of PSII is also analyzed in the next Section 4.2. First, there is almost no increase of slowly-decaying component in heterocyst by the increase of laser power (Table 2, Figs. 2(b), (c), S3, S4). Even in the selected subset of heterocysts (subset/w) (Table 2), the increase of the long-lived component at 689 nm is from 8% to at most 12% in the amplitude while the corresponding long-lived component in vegetative cells increases in the amplitude from 2.5% to 37% between 0.08 and 20 nW. Second, the CFLs at both 689 and 716 nm in heterocyst are clearly shorter than those in vegetative cells (Table 1). This reflects higher abundance of PSI in heterocyst as CFL of PSI is widely reported to be shorter than that of PSII [18,28,36,77]. Third, the CFL at 689 nm of heterocyst is shorter than that at 716 nm. This is in contrast to the very similar CFL of the short-lived component (0.22–0.26 ns) in the vegetative cells between 689 and 716 nm (Table 1). This feature is consistent with the observation in purified PSI complexes (PSI or PSI–LHCI) or in mutants lacking PSII and its associated antenna system, in which there are one relatively fast decay around the main peak of the Qy band (major spectral forms of Chla in PSI, with fluorescence wavelength <700 nm) and one relatively slow decay of the so-called minor long-wavelength-absorbing form (>700 nm) [36,77]. For example, one of the above-cited time-resolved spectroscopic study reported two main fluorescence decay lifetimes of 15 ps and 50 ps that are attributable to net loss of fluorescence (trapping) in isolated PSI from a cyanobacterium *Spirulina platensis* [77]. In their work, the fast trapping component (15 ps) is centered around 700 nm with an approximate FWHM of 46 nm, whereas the slow component (50 ps) is centered around 730 nm with an approximate FWHM of 57 nm. Although our IRFs (0.08 ns at 689 nm and 0.10 ns at 716 nm in FWHM) and the signal-to-noise ratio are presumably not sufficient to resolve the two trapping components at a single wavelength alone, the relatively slow decay at 716 nm (0.13–0.14 ns) than at 689 nm (0.084–0.096 ns) of the CF in heterocyst is most plausibly attributable to the presence of the two trapping dynamics with different spectra and lifetimes in PSI. This trend would not be easily observed if there was a substantial contribution from PSII to the wavelength region around the main Qy peak (around 689 nm), as the CFL of PSII is generally even slower than the slow trapping component in PSI.

Contribution of PSI in the vegetative cells of *A. variabilis* is noticeable as a decreased amplitude of the long-lived CF due to closed PSII around 716 nm (16% at 20 nW) than that around 689 nm (37% at 20 nW in Table 1). The decreased amplitude of the long-lived component at 716 nm than at 689 nm can be at least in part attributable to higher spectral weight of PSI at 716 nm than at 689 nm. Contribution of PSI in *P. kessleri* was also noticeable in the varied amplitude of the long-lived components (28% at 716 nm vs. 53% at 689 nm with 1.0×10^3 pW in Table 3). These suggest that not only the dependence of FL on laser power but also dual-wavelength detection can be helpful for imaging PSI/PSII.

4.2. Long-lived fluorescence and possible presence of PSII in heterocysts

In one selected subset of heterocysts (subset/w, 5 among 22 heterocysts), a long-lived fluorescence with a lifetime of 0.57–0.74 ns was found with a substantial amplitude larger than 8% at all laser intensities (Table 2, Fig. S4). However, its increase in amplitude by the rise of laser power was only from 8 to at most 12% (Table 2, Fig. S4), which is about one-order of magnitude smaller than that in vegetative cells (from 2.5 to 37%, Table 1). The amplitude of 8% at the weakest excitation should be thus attributed to long-lived fluorescence other than closed PSII. One possibility is that these indicate phycobilisomes or parts of phycobilisomes that are uncoupled from both PSII and PSI [78]. In our random selection of heterocysts, it is impossible to avoid premature heterocysts, which temporarily contain substantial number of uncoupled highly fluorescent phycobilisome [9,49,79]. Given this possibility, the small increase of the long-lived component from 8 to 11–12% in the subset of heterocyst (subset/w) by the rise of laser intensity (Table 2) may also be attributable not to stable presence of functional PSII but to residual but photochemically active PSII that is not yet decomposed during the heterocyst differentiation. It should be noted that the substantial amplitude of the long-lived component was observed only in the minor subset (subset/w): 3 heterocysts in filaments harvested 24 days after the inoculation (total was 9 heterocysts), 2 heterocysts in filaments harvested 90 days after the inoculation (total was 6 heterocysts), and none in filaments harvested 3 days after the inoculation (total was 7 heterocysts). All these inoculations were *not* step-down of the nitrogen, but simply dilutions of cells from cell-rich nitrogen-deficient media to new nitrogen-deficient media. As far as randomly sampled 22 heterocysts in this study are concerned, we tentatively estimated that photochemically active PSII:PSI ratio in heterocysts are estimated to be typically below our detection limit and at most about 5% in limited cases in comparison with that in vegetative cells (See Text S3 for the details of this estimation). This number was given on an assumption that effective light-harvesting abilities of PSII in vegetative cells and heterocysts are the same under the experimental conditions in this work (state II and 404 nm excitation). To further clarify the molecular entity of the long-lived fluorescence, it is thus desirable to carry out a FLIM-based time-lapse observation on heterocyst differentiation, which will be described in our next publications.

4.3. Fluorescence lifetime when PSII is in the open state

Most obvious mission of FLIM should be to obtain absolute values of CFLs in a wide spatial region including three dimensional objects like plant leaves. Straightforward comparison of CFLs between different organisms or different cells is generally meaningful, but only when CFLs to be compared should be obtained at well-defined excitation and preillumination conditions, e.g., at weak excitation limits after dark adaptation that are generally attained at different laser powers for different organisms/tissues, as demonstrated in Fig. 4. The average FL at 689 nm seems to reach a weak limit below 0.30 nW and 55 pW in the cases of *A. variabilis* vegetative cells and *P. kessleri* cells, respectively (Tables 1 and 3, Fig. 4), although double exponential curve fitting did not give constant results due probably to the limited s/n ratio in the relatively weak excitation powers. The average FL with PSII in the open state thus seems to be 0.25 ns and 0.36–0.39 ns in the cases of *A. variabilis* vegetative cells and *P. kessleri* cells, respectively, which are largely consistent with previous reports (Tables S5, S6). Even if the primary charge separation in the isolated core PSII dimer is intrinsically common between *P. kessleri* and *A. variabilis*, the different CFLs between *A. variabilis* and *P. kessleri* at the weak limit (0.25 and 0.36–0.39 ns, respectively) observed in this study can be caused by the difference in the organization of light-harvesting system. With the 404 nm excitation in our PSII models, 63% and 26% of the excitation at 404 nm is estimated to initially reside in the PSII dimer in *A. variabilis* and *P. kessleri*, respectively (Table S7 and S8), when any excitation in the whole PSII supercomplex including associated phycobilisome is set to be 100%. In addition, back

energy transfer from the PSII dimer to light-harvesting systems in the *P. kessleri* (PSII → LHCII, CP26 and CP29) seems to be far more significant than that in *A. variabilis* (PSII → APC, PC, PEC). This is supported by the estimation of number of pigments weighted by the thermal excitation probability in both the core PSII dimer and associated light-harvesting systems (Tables S7 and S8). It should be also noted that PBS tends to be associated with PSI rather than with PSII in the dark-adapted state (state 2 in the case of cyanobacteria) [2,62,63]. It thus seems very reasonable that average FL at the weak limit in *A. variabilis* is shorter than in *P. kessleri* upon the 404 nm excitation. However, it should be certainly noted that contribution of PSI, which has a CFL of largely 0.08–0.09 ns at 689 nm in heterocyst in *A. variabilis* (Table 2), should also make the apparent CFL of vegetative cells around 689 nm shorter than that of pure PSII to some extent. The contribution of PBS to the lifetime of vegetative cells of *A. variabilis* at 689 nm is likely less substantial than that of PSI, since substantial part of PBS is dissociated from PSII by the state II conditions and the excitation wavelength at 404 nm is more preferential for Chla than phycobilin (Table S7).

4.4. Transition from open to closed state of PSII as observed by varied excitation laser power

The transition from open to closed state in the majority of PSII of *A. variabilis* is observed at about one-order of magnitude higher excitation power than that of *P. kessleri*. The recovery dynamics of open PSII from closed PSII in cyanobacteria (0.22 ms (68%), 2.9 ms (23%) and 13 s (9%) in *Synechocystis* sp. PCC 6803 [55]) seems to be largely similar to that in green algae (0.23 ms (73%), 46 ms (16%) and 7.5 s (11%) in *C. reinhardtii* [56]). The difference in the laser power necessary to close most PSII thus seems to be primarily attributable to the difference in the absorption coefficient at 404 nm for PSII. In *P. kessleri*, as one of green algae, PSII possess an antenna system that contains Chla and chlorophyll *b* (Chlb) as main antenna pigments exhibiting strong absorption mainly in the blue-green and red regions [80,81]. For the simulation, we have assumed the same molecular organization of PSII supercomplex as in *C. reinhardtii* [67], the total absorption coefficient per PSII monomer in state 1 (Text S2) is equivalent to about 191 Chla molecules per monomer PSII (Fig. 4(b)). The simulation curve for the light-harvesting ability equivalent to 380 Chla may give a slightly improved fit to the experiment. Absolute absorption cross section of PSII in *Chlorella vulgaris* was reported to be equivalent to 130–400 Chla [72]. It should be also noted that there remains a certain long-lived component (≥0.6 ns) even at the weak limit, which is similar to the situations in some references reporting such minor long-lived component (See Table S5 for references) [26,35]. Given this possibility, the estimated ratio of closed PSII based on the amplitude of the long-lived component (closed circles in Fig. 4(b)) may have to be modified. On an assumption that 12% of the amplitude at zero time (the amplitude of the 0.82 ns component at 689 nm, 4 pW in Table 3) is intrinsically given by the open PSII, our experimental data yield another plot for the ratio of closed PSII (open circles) in Fig. 4(b). This modified experimental plot matches well with the simulation. In the case of *A. variabilis*, the experiment was best reproduced by the simulation if all PBS components are dissociated from PSII and if PSI contribute to the short-lived component (≤0.23 ns) at 689 nm by about 33% in the amplitude ratio at t = 0 ps (the simulation curve: PSII alone × (2/3) in Fig. 4(a)), as explained in Section 3.2.

The rise in FL with the increase of laser power is sensitively influenced by both the antenna size of PSII and recovery dynamics of open PSII from its closed states (Fig. S8(b)). Although the two factors of antenna size and the recovery rate of open PSII are inseparable in the input-power dependence of FLIM alone, FLIM will be certainly helpful for obtaining a new type of images on antenna size and/or recovery rate of open PSII. For example, about 3–4 cells near the heterocyst cell in *A. variabilis* (part A of the filament in Fig. 1(f)) show an average FL of about 0.25 ns, and about 2 cells in the same filament (part B of the filament in Fig. 1(f)) show an average FL of about 0.4 ns at the same excitation power. Such a difference is not yet generalized, but it may suggest differently regulated light-harvesting abilities and/or redox conditions of plastoquinone pool affecting electron transfers from Q_A [53,64]. Properties of individual vegetative cells as well as heterocysts will be analyzed based on FLIM data in our next publications.

4.5. Relevance of FLIM to PAM parameters

Pulse-amplitude-modulation fluorometry (PAM) of CF is probably the most popular chlorophyll fluorometry on photosynthetic organisms [51,52]. There have been extensive reports demonstrating microscopic images for PAM-related parameters from individual chloroplasts and cyanobacterial cells [5,82–85]. FLIM data with varied excitation power also contains information directly related to the PAM. Since the simulation based on open-closed status of PSII in this study largely reproduced the experimental results in terms of ratio of closed PSII included in the FLIM data (Fig. 4), the maximum yield of PSII charge separation under dark-adapted chloroplasts or cyanobacteria in PAM analysis is related to the CFL as follows.

$$\frac{\langle\tau_{open}\rangle^{-1}-{\tau_{closed}}^{-1}}{\langle\tau_{open}\rangle^{-1}}=\frac{(0.38)^{-1}-(1.42)^{-1}}{(0.38)^{-1}}=0.73 \quad (6)$$

for *P. kessleri* (cf. Table 3, Text S6, Fig. S7).

$$\frac{\langle\tau_{open}\rangle^{-1}-{\tau_{closed}}^{-1}}{\langle\tau_{open}\rangle^{-1}}=\frac{(0.25)^{-1}-(0.75)^{-1}}{(0.25)^{-1}}=0.67 \quad (7)$$

for vegetative cells of *A. variabilis*.
(cf. Table 1, Text S6).

The above $<\tau_{open}>$ and τ_{closed} are set to be the average fluorescence lifetime at 689 nm at the weakest laser power and the time constant of the slowly-decaying component at 689 nm at the highest laser power, respectively. In the above estimation, we assume that the average fluorescence lifetime at a sufficiently high laser power to close all PSII should be equal to the CFL of the most long-lived component that we observed. In the case of *P. kessleri*, this value is slightly lower than the typical value of $(F_M - F_0) / F_M = F_V/F_M$ (about 0.8) in dark-adapted state in the PAM fluoromerty on green algae including *Chlorella* [62,86], although the two values should be ideally the same in the simple two-state model (Text S6). Possible activation of protective quenching against excess excitation (so-called nonphotochemical quenching, NPQ) during the scanning laser illumination may decrease the apparent maximum yield of PSII charge separation through shortening of τ_{closed}. However, such a scenario is unlikely in this study, because the average intensity of the excitation laser at 1 nW (strongest laser power in the consecutive FLIM measurements in the case of *P. kessleri* summarized in Table 3) for 45 × 45 μm scanning area is estimated to be about 1.7 μmol photons $m^{-2}s^{-1}$ (Text S4). This is about one or two order of magnitude smaller than that used for actinic light in most PAM measurements to induce NPQ [51,52]. Moreover, consecutive FLIM measurements for a total exposure time of 45 s at even higher excitation laser at 6 nW (the other experimental conditions are unchanged from those used in the results of the main text) did not show noticeable changes in CF decay profile from the first 4.5 s to the last 4.5 s in the case of *P. kessleri* cells (Fig. S7). The above discrepancy in the maximum quantum yield (between 0.73 and about 0.8) may suggest an underestimation of the amplitude of some short-lived component in the fluorescence decay due to our limited time-resolution (FWHM of IRF was 80 ps at 689 nm) and/or s/n. On the other hand, the above value of $(<\tau_{open}>^{-1} - \tau_{closed}^{-1}) / \tau_{open}^{-1}$ is higher than typical values of F_V/F_M of dark-adapted cyanobacteria [53,62,64]. This is caused by the contribution of at least PSI and also PBS to the short lifetime component with the FL of about 0.23 ns (See Section 3.2 and Fig. 4(a)). The PSI/PSII ratio in cyanobacteria are generally higher than those in green

algae [57]. It is thus likely that CFL of pure PSII is longer than 0.25 ns in *A. variabilis*. For a direct comparison with actual PAM measurements on cyanobacteria, τ_{closed} in Eq. (7) may have to be replaced with $<\tau_{closed}>$ as follows.

$$\frac{\langle\tau_{open}\rangle^{-1}-\langle\tau_{closed}\rangle^{-1}}{\langle\tau_{open}\rangle^{-1}}=\frac{(0.25)^{-1}-(0.44)^{-1}}{(0.25)^{-1}}=0.43 \quad (8)$$

for vegetative cells of *A. variabilis*.
(cf. Table 1, Text S6).

$$\frac{\langle\tau_{open}\rangle^{-1}-\langle\tau_{closed}\rangle^{-1}}{\langle\tau_{open}\rangle^{-1}}=\frac{(0.087)^{-1}-(0.129)^{-1}}{(0.087)^{-1}}=0.33 \quad (9)$$

for all 22 heterocysts of *A. variabilis*.
(cf. Table 2, Text S6).

These are comparable to and largely consistent with the values of F_V/F_M reported for vegetative cells and heterocysts in *Anabaena* sp. strain PCC7120 by time-lapse microscopic PAM (or fluorescence kinetic microscopy, FKM) [5]. The estimation on heterocysts based on our results, however, critically depends on the two subsets, subset/w/o and subset/w, for which the Eq. (9) gives 0.07 and 0.27 based on Table 2, respectively. According to the time-dependent F_V/F_M values after the nitrogen step-down in the reference [5], the value of 0.07 for the subset/w/o corresponds to a late "stress period" (about 30 h after the nitrogen step-down). The value of 0.27 for the subset/w corresponds to an early "stress period" (about 20–25 h after the nitrogen step-down) or "acclimation period" (about 120 h after the nitrogen step-down). In the former case, the relatively minor subset of heterocysts (subset/w having a substantial long-lived fluorescence) is indeed understandable as a transient state during the heterocyst development. However, it should be noted that our estimation is critically dependent on the accuracy of the curve fitting at the weak excitation limit and that we need to increase the number of sampling in order to reach a definite conclusion.

4.6. Limitations of current simulation model and data analysis

Some previous studies have suggested a need to introduce the so-called three-state model of the charge separation assuming open, semi-closed, and closed states, which reflect redox states of at least two sequential electron acceptors (Text S5) [87,88]. Semi-closed state is suggested to show lower fluorescence quantum yield than that in fully closed state [87], which may be consistently observed in this study as the slightly shorter CFLs of the "closed" state at the medium laser powers (0.63–0.82 ns at 4–265 pW in *P. kessleri*) than those at the highest laser power (1.24–1.42 ns at 1.0–6.0 × 10^3 pW in *P. kessleri*) (Table 3, Fig. S5). The need for the three-state model is also supported by the residuals and chi square values of the curve fitting in Figs. S2 – S5, which show that the single or double exponential function are sufficient only at weak - medium excitation powers that we employed. The presence of more than two exponential components at the relatively high laser powers should be explained in an improved model in our next publications.

Moreover, even at low laser powers where most PSII are open, the intrinsic fluorescence decay of PSII is generally multiexponential with at least 3–5 lifetimes in both green algae [25,31,35] and cyanobacteria [36,45–47] especially when the decay of CF is observed from many cells by non-FLIM TCSPC with a high s/n (See also Tables S5, S6). The sufficiency of single or double components especially at the relatively weak laser powers in our case is just given by our limited s/n. The relatively low s/n is inevitable as far as we primarily concern imaging in order to resolve individual cells within a short time. Our contribution is thus focusing on the overall reproduction of the experimental results, which are approximately described as sum of at most two exponential functions at all power levels, by the relatively crude but elaborate two-state model for the PSII status. Improvement of the simulation model together with the more accurate analysis on the experimental results will be carried out in our next studies with more focus on differences between individual cells.

4.7. Comparison with other FLIM studies in terms of open-closed status of PSII and laser power dependence

A brief overview is given to the laser power levels and/or excitation probabilities that are employed in previously reported FLIM-based imaging of chloroplasts and cyanobacteria. In some cases, NPQ processes were mainly studied at light levels that seem to close substantial fraction of PSII [14,16]. In one of the studies [16], the major CFL in avocado plants was about 1.5 ns (probably from closed PSII) and activation of NPQ was observed as appearance of CFL around 0.5 ns. A certain oligomeric state of LHCII was suggested to show a CFL of 0.4 ns when NPQ was induced in *Arabidopsis* leaves [89]. In other cases, average CFL was found to be in the range between 0.15 and 0.5 ns at relatively weak laser power [15,21,36,90]. On the other hand, CF with two-photon excitation has been reported to decrease in lifetime by raising incident laser power [18,19], which has been ascribed to singlet–singlet and/or singlet–triplet annihilation. This is a qualitatively different trend than those reported with visible excitation including this work [34]. Singlet–singlet annihilation can be operative only when a single laser pulse excites multiple pigments in the same or nearby PSII unit(s) among which at least multi-step energy transfer to each other is possible, because typical pulse-to-pulse interval of about 10 ns or longer (13.2 ns in this work) is sufficiently longer than lifetime of fluorescence (lifetime of singlet excited state of Chls). Our estimation of the excitation probability of PSII in *P. kessleri* by a single laser pulse of 1 nW power (at 404 nm, and highest laser power in Table 3) is only about 5×10^{-3}, by which singlet–singlet annihilation should be virtually negligible (Text S5). If prepared concentration of excited PSII at the focus and detection efficiency of CF in the references ([18,19]) are comparable to our conditions, singlet–singlet annihilation can thus be safely excluded. Singlet–triplet annihilation may be operative, since formation of triplet state(s) of Chls and/or carotenoids is certainly enhanced when substantial portion of PSII is closed at high input laser power and their lifetimes are in the range of μs to ms [91–94]. The long-lived triplet states may thus interact with singlet excited state prepared in the subsequent laser pulses, which leads to shortening of fluorescence lifetime. Lifetime shortening in the FLIM by NPQ and singlet–triplet annihilation may be differentiated on a more quantitative basis if one performs a numerical simulation to estimate the transient accumulation of the triplet states during FLIM imaging, as shown in this work.

5. Conclusions

FLIM data of a single cellular green alga *P. kessleri* and nitrogen-fixing filamentous cyanobacterium *A. variabilis* were obtained at varied excitation powers. At weak excitation limits, fluorescence lifetimes of the thylakoid membrane with mostly open PSII can be obtained, although it takes a long total exposure time to obtain a high quality image. The transition in FLIM data from the weak excitation limits to higher powers that close a substantial fraction of PSII can be successfully explained by a numerical model considering the open-closed status of PSII based on absolute laser powers. The difference in FLIM between *P. kessleri* and cyanobacterium *A. variabilis* can be largely explained by the difference in the light-harvesting ability of the PSII supercomplex at the excitation wavelength at 404 nm. The fluorescence decay in nitrogen-fixing heterocysts is largely independent of the excitation power. This reflects a high purity of PSI in the unique heterocyst thylakoid lacking PSII. Among heterocysts that were randomly sampled, photochemically active PSII/PSI ratio in heterocysts is at most about 5% in comparison with that of vegetative cells. Heterogeneous properties of individual heterocysts were found, but accurate determination of their physiological states should await further studies.

A whole plant leaf can be a target of FLIM, but special care should be taken when comparing chloroplasts in deep regions with those close to the surface, because it is in general difficult to estimate absolute laser power reaching deep individual chloroplasts. The dependence of FLIM on laser power is sensitively influenced by at least the antenna size of PSII and recovery rates of open PSII from its closed states. A simulation fully reflecting laser scanning conditions, as shown in this work, will potentially help one to interpret observed features of FLIM images in terms of important parameters of photochemistry in individual chloroplasts, cyanobacterial cells and thylakoid domains.

Funding

This work was supported in part by the Japan Science and Technology Agency (the Precursory Research for Embryonic Science and Technology, "Chemical conversion of light energy", to S.K.), the Ministry of Education, Culture, Sports, Science and Technology in Japan (MEXT) (grant no. 24,657,036 to T. S. & S.K.), MEXT-Supported Program for the Strategic Research Foundation at Private Universities (2015–2018, no. S1511025 partly to S.K.), the Murata Science Foundation (to S.K.), and Shorai Foundation for Science and Technology (to S.K.).

Disclosures

Dr. Kumazaki reports grants and personal fees from Japan Science and Technology Agency, grants from The Murata Science Foundation, grants from Shorai Foundation for Science and Technology, grants from the Ministry of Education, Culture, Sports, Science and Technology in Japan during the conduct of the study.

Transparency document

The Transparency document associated with this article can be found, in online version.

Acknowledgments

We thank Profs. Haruo Inoue (Tokyo Metropolitan University) for many valuable advice and Mr. Masashi Akari, Mr. S. Fukuda, Mr. K. Tamamizu, Mr. K. Kodama for their contributions at preliminary stages of this work.

Appendix A supplementary data

Supplementary data to this article can be found online at http://dx.doi.org/10.1016/j.bbabio.2015.10.003.

References

[1] Govindjee, Chlorophyll a fluorescence: a bit of basics and history, in: C. Papageorgiou, Govindjee (Eds.), Chlorophyll a Fluorescence a Signature of Photosynthesis, Springer, Netherland 2004, pp. 1–42.
[2] G.C. Papageorgiou, M. Tsimilli-Michael, K. Stamatakis, The fast and slow kinetics of chlorophyll a fluorescence induction in plants, algae and cyanobacteria: a viewpoint, Photosynth. Res. 94 (2007) 275–290.
[3] V. Sarafis, Chloroplasts: a structural approach, J. Plant Physiol. 152 (1998) 248–264.
[4] K. Harter, A.J. Meixner, F. Schleifenbaum, Spectro-microscopy of living plant cells, Mol. Plant 5 (2012) 14–26.
[5] N. Ferimazova, K. Felcmanova, E. Setlikova, H. Kupper, I. Maldener, G. Hauska, B. Sediva, O. Prasil, Regulation of photosynthesis during heterocyst differentiation in anabaena sp strain PCC 7120 investigated in vivo at single-cell level by chlorophyll fluorescence kinetic microscopy, Photosynth. Res. 116 (2013) 79–91.
[6] W.F.J. Vermaas, J.A. Timlin, H.D.T. Jones, M.B. Sinclair, L.T. Nieman, S.W. Hamad, D.K. Melgaard, D.M. Haaland, In vivo hyperspectral confocal fluorescence imaging to determine pigment localization and distribution in cyanobacterial cells, Proc. Natl. Acad. Sci. U. S. A. 105 (2008) 4050–4055.
[7] M. Hasegawa, T. Shiina, M. Terazima, S. Kumazaki, Selective excitation of photosystems in chloroplasts inside plant leaves observed by near-infrared laser-based fluorescence spectral microscopy, Plant Cell Physiol. 51 (2010) 225–238.
[8] M. Hasegawa, T. Yoshida, M. Yabuta, M. Terazima, S. Kumazaki, Anti-stokes fluorescence spectra of chloroplasts in parachlorella kessleri and maize at room temperature as characterized by near-infrared continuous-wave laser fluorescence microscopy and absorption microscopy, J. Phys. Chem. B 115 (2011) 4184–4194.
[9] S. Kumazaki, M. Akari, M. Hasegawa, Transformation of thylakoid membranes during differentiation from vegetative cell into heterocyst visualized by microscopic spectral imaging, Plant Physiol. 161 (2013) 1321–1333.
[10] K. Sugiura, S. Itoh, Single-cell confocal spectrometry of a filamentous cyanobacterium nostoc at room and cryogenic temperature. Diversity and differentiation of pigment systems in 311 cells, Plant Cell Physiol. 53 (2012) 1492–1506.
[11] E. Kim, T.K. Ahn, S. Kumazaki, Changes in antenna sizes of photosystems during state transitions in granal and stroma-exposed thylakoid membrane of intact chloroplasts in arabidopsis mesophyll protoplasts, Plant Cell Physiol. 56 (2015) 759–768.
[12] Y. Shibata, W. Katoh, Y. Tahara, Study of cell-differentiation and assembly of photosynthetic proteins during greening of etiolated Zea mays leaves using confocal fluorescence microspectroscopy at liquid-nitrogen temperature, Biochim. Biophys. Acta Bioenerg. 1827 (2013) 520–528.
[13] C.A. Buecherl, A. Bader, A.H. Westphal, S.P. Laptenok, J.W. Borst, FRET–FLIM applications in plant systems, Protoplasma 251 (2014) 383–394.
[14] O. Holub, M.J. Seufferheld, C.G. Govindjee, G.J. Heiss, R.M. Clegg, Fluorescence lifetime imaging microscopy of *Chlamydomonas reinhardtii*: non-photochemical quenching mutants and the effect of photosynthetic inhibitors on the slow chlorophyll fluorescence transient, J. Microsc. (Oxford) 226 (2007) 90–120.
[15] M. Iwai, M. Yokono, N. Inada, J. Minagawa, Live-cell imaging of photosystem II antenna dissociation during state transitions, Proc. Natl. Acad. Sci. U. S. A. 107 (2010) 2337–2342.
[16] S. Matsubara, Y.-.C. Chen, R. Caliandro, Govindjee, R.M. Clegg, Photosystem II fluorescence lifetime imaging in avocado leaves: contributions of the lutein-epoxide and violaxanthin cycles to fluorescence quenching, J. Photochem. Photobiol. B Biol. 104 (2011) 271–284.
[17] C. Unlu, B. Drop, R. Croce, H. van Amerongen, State transitions in *Chlamydomonas reinhardtii* strongly modulate the functional size of photosystem II but not of photosystem I, Proc. Natl. Acad. Sci. U. S. A. 111 (2014) 3460–3465.
[18] K. Broess, J.W. Borst, H. van Amerongen, Applying two-photon excitation fluorescence lifetime imaging microscopy to study photosynthesis in plant leaves, Photosynth. Res. 100 (2009) 89–96.
[19] Y. Zeng, Y. Wu, D. Li, W. Zheng, W.X. Wang, J.N.Y. Qu, Two-photon excitation chlorophyll fluorescence lifetime imaging: a rapid and noninvasive method for in vivo assessment of cadmium toxicity in a marine diatom thalassiosira weissflogii, Planta 236 (2012) 1653–1663.
[20] Y. Wu, Y. Zeng, J.A.Y. Qu, W.X. Wang, Mercury effects on thalassiosira weissflogii: applications of two-photon excitation chlorophyll fluorescence lifetime imaging and flow cytometry, Aquat. Toxicol. 110 (2012) 133–140.
[21] A.S. Kristoffersen, O. Svensen, N. Ssebiyonga, S.R. Erga, J.J. Stamnes, O. Frette, Chlorophyll a and NADPH fluorescence lifetimes in the microalgae *Haematococcus pluvialis* (chlorophyceae) under normal and astaxanthin-accumulating conditions, Appl. Spectrosc. 66 (2012) 1216–1225.
[22] T. Kolubayev, N.E. Geacintov, G. Paillotin, J. Breton, Domain sizes in chloroplasts and chlorophyll–protein complexes probed by fluorescence yield quenching induced by singlet–triplet exciton annihilation, Biochim. Biophys. Acta 808 (1985) 66–76.
[23] V. Barzda, V. Gulbinas, R. Kananavicius, V. Cervinskas, H.V. Amerongen, R.V. Grondelle, L. Valkunas, Singlet–singlet annihilation kinetics in aggregates and trimers of LHCII, Biophys. J. 80 (2001) 2409–2421.
[24] V. Barzda, C.J. de Grauw, J. Vroom, F.J. Kleima, R. van Grondelle, H. van Amerongen, H.C. Gerritsen, Fluorescence lifetime heterogeneity in aggregates of LHCII revealed by time-resolved microscopy, Biophys. J. 81 (2001) 538–546.
[25] R.J. Gulotty, L. Mets, R.S. Alberte, G.R. Fleming, Picosecond fluorescence study of photosynthetic mutants of chlamydomonas reinhardii: origin of the fluorescence decay kinetics of chloroplasts, Photochem. Photobiol. 41 (1985) 487–496.
[26] A.R. Holzwarth, J. Wendler, W. Haehnel, Time-resolved picosecond fluorescence spectra of the antenna chlorophylls in *Chlorella vulgaris*. Resolution of photosystem I fluorescence, Biochim. Biophys. Acta Bioenerg. 807 (1985) 155–167.
[27] I. Moya, M. Hodges, J. Briantais, G. Hervo, Evidence that the variable chlorophyll fluorescence in *Chlamydomonas reinhardtii* is not recombination luminescence, Photosynth. Res. 10 (1986) 319–325.
[28] G.H. Krause, E. Weis, Chlorophyll fluorescence and photosynthesis — the basics, Annu. Rev. Plant Physiol. Plant Mol. Biol. 42 (1991) 313–349.
[29] H.J. Keuper, K. Sauer, Effect of photosystem II reaction center closure on nanosecond fluorescence relaxation kinetics, Photosynth. Res. 20 (1989) 85–103.
[30] K. Amarnath, J. Zaks, S.D. Park, K.K. Niyogi, G.R. Fleming, Fluorescence lifetime snapshots reveal two rapidly reversible mechanisms of photoprotection in live cells of *Chlamydomonas reinhardtii*, Proc. Natl. Acad. Sci. U. S. A. 109 (2012) 8405–8410.
[31] F. Rizzo, G. Zucchelli, R. Jennings, S. Santabarbara, Wavelength dependence of the fluorescence emission under conditions of open and closed Photosystem II reaction centres in the green alga *Chlorella sorokiniana*, Biochim. Biophys. Acta Bioenerg. 1837 (2014) 726–733.
[32] F. Franck, P. Juneau, R. Popovic, Resolution of the photosystem I and photosystem II contributions to chlorophyll fluorescence of intact leaves at room temperature, Biochim. Biophys. Acta Bioenerg. 1556 (2002) 239–246.
[33] N. Moise, I. Moya, Correlation between lifetime heterogeneity and kinetics heterogeneity during chlorophyll fluorescence induction in leaves: 1. Mono-frequency phase and modulation analysis reveals a conformational change of a PSII pigment complex during the IP thermal phase, Biochim. Biophys. Acta Bioenerg. 1657 (2004) 33–46.
[34] L.J. Tian, S. Farooq, H. van Amerongen, Probing the picosecond kinetics of the photosystem II core complex in vivo, Phys. Chem. Chem. Phys. 15 (2013) 3146–3154.
[35] J. Wendler, A.R. Holzwarth, State transitions in the green alga *Scenedesmus obliquus* probed by time-resolved chlorophyll fluorescence spectroscopy and global data analysis, Biophys. J. 52 (1987) 717.

[36] S.B. Krumova, S.P. Laptenok, J.W. Borst, B. Ughy, Z. Gombos, G. Ajlani, H. van Amerongen, Monitoring photosynthesis in individual cells of synechocystis sp. PCC 6803 on a picosecond timescale, Biophys. J. 99 (2010) 2006–2015.
[37] R. Haselkorn, Heterocysts, Annu. Rev. Plant Physiol. Plant Mol. Biol. 29 (1978) 319–344.
[38] R. Grotjohann, M.S. Rho, W. Kowallik, Influences of blue and red-light on the photosynthetic apparatus of *Chlorella kessleri* — alterations in pigment–protein complexes, Bot. Acta 105 (1992) 168–173.
[39] I. Ikegami, A. Kamiya, Presence of the photoactive reaction-center chlorophyll of PSI (P700) in dark-grown cells of a chlorophyll-deficient mutant of *Chlorella kessleri*, Plant Cell Physiol. 39 (1998) 1087–1092.
[40] S.Y. Ow, T. Cardona, A. Taton, A. Magnuson, P. Lindblad, K. Stensjo, P.C. Wright, Quantitative shotgun proteomics of enriched heterocysts from nostoc sp. PCC 7120 using 8-plex isobaric peptide tags, J. Proteome Res. 7 (2008) 1615–1628.
[41] T. Cardona, N. Battchikova, P. Zhang, K. Stensjo, E.M. Aro, P. Lindblad, A. Magnuson, Electron transfer protein complexes in the thylakoid membranes of heterocysts from the cyanobacterium nostoc punctiforme, Biochim. Biophys. Acta 1787 (2009) 252–263.
[42] J.-J. Park, S. Lechno-Yossef, C.P. Wolk, C. Vieille, Cell-specific gene expression in *Anabaena variabilis* grown phototrophically, mixotrophically, and heterotrophically, BMC Genomics 14 (2013).
[43] R.Y. Stanier, R. Kunisawa, M. Mandel, G. Cohenbaz, Purification and properties of unicellular blue–green algae (Order Cchroococcales), Bacteriol. Rev. 35 (1971) 171.
[44] E. Bittersmann, A. Holzwarth, G. Agel, W. Nultsch, Picosecond time-resolved emission spectra of photoinhibited and photobleached *Anabaena variabilis*, Photochem. Photobiol. 47 (1988) 101–105.
[45] E. Bittersmann, W. Vermaas, Fluorescence lifetime studies of cyanobacterial photosystem II mutants, Biochim. Biophys. Acta Bioenerg. 1098 (1991) 105–116.
[46] C.W. Mullineaux, A.R. Holzwarth, Effect of photosystem II reaction centre closure on fluorescence decay kinetics in a cyanobacterium, Biochim. Biophys. Acta Bioenerg. 1183 (1993) 345–351.
[47] J. Veerman, F.K. Bentley, J.J. Eaton-Rye, C.W. Mullineaux, S. Vasil'ev, D. Bruce, The PsbU subunit of photosystem II stabilizes energy transfer and primary photochemistry in the phycobilisome-photosystem II assembly of synechocystis sp. PCC 6803, Biochemistry 44 (2005) 16939–16948.
[48] L. Ying, X. Huang, B. Huang, J. Xie, J. Zhao, X.S. Zhao, <Ying_2002_Anabaena_sp PCC7120_spectral_confocal.pdf>, Photochem. Photobiol. 76 (2002) 310–313.
[49] S. Ke, R. Haselkorn, Fluorescence spectroscopy study of heterocyst differentiation in Anabaena PCC 7120 filaments, Microbiology-SGM 159 (2013) 253–258.
[50] S.W. Hogewoning, E. Wientjes, P. Douwstra, G. Trouwborst, W. van Ieperen, R. Croce, J. Harbinson, Photosynthetic quantum yield dynamics: from photosystems to leaves, Plant Cell 24 (2012) 1921–1935.
[51] K. Roháček, M. Barták, Technique of the modulated chlorophyll fluorescence: basic concepts, useful parameters, and some applications, Photosynthetica 37 (1999) 339–363.
[52] U. Schreiber, Pulse-amplitude-modulation (PAM) fluorometry and saturation pulse method: an overview, Chlorophyll a Fluorescence, Springer 2004, pp. 279–319.
[53] D. Campbell, V. Hurry, A.K. Clarke, P. Gustafsson, G. Oquist, Chlorophyll fluorescence analysis of cyanobacterial photosynthesis and acclimation, Microbiol. Mol. Biol. Rev. 62 (1998) 667.
[54] K. El Bissati, D. Kirilovsky, Regulation of psbA and psaE expression by light quality in Synechocystis species PCC 6803. A redox control mechanism, Plant Physiol. 125 (2001) 1988–2000.
[55] I. Vass, D. Kirilovsky, A.L. Etienne, UV-B radiation-induced donor- and acceptor-side modifications of photosystem II in the cyanobacterium synechocystis sp PCC 6803, Biochemistry 38 (1999) 12786–12794.
[56] A. Volgusheva, G. Kukarskikh, T. Krendeleva, A. Rubin, F. Mamedov, Hydrogen photoproduction in green algae *Chlamydomonas reinhardtii* under magnesium deprivation, RSC Adv. 5 (2015) 5633–5637.
[57] Y. Hihara, K. Sonoike, Regulation, inhibition and protection of photosystem I, Regulation of Photosynthesis, Springer 2001, pp. 507–531.
[58] Y. Umena, K. Kawakami, J.-R. Shen, N. Kamiya, Crystal structure of oxygen-evolving photosystem II at a resolution of 1.9 Å, Nature 473 (2011) 55–60.
[59] T. Watanabe, A. Hongu, K. Honda, M. Nakazato, M. Konno, S. Saitoh, Preparation of chlorophylls and pheophytins by isocratic liquid-chromatography, Anal. Chem. 56 (1984) 251–256.
[60] E.W. Chappelle, M.S. Kim, J.E. McMurtrey, Ratio analysis of reflectance spectra (rars) — an algorithm for the remote estimation of the concentrations of chlorophyll-a, chlorophyll-b, and carotenoids in soybean leaves, Remote Sens. Environ. 39 (1992) 239–247.
[61] S.L. Ustin, A.A. Gitelson, S. Jacquemoud, M. Schaepman, G.P. Asner, J.A. Gamon, P. Zarco-Tejada, Retrieval of foliar information about plant pigment systems from high resolution spectroscopy, Remote Sens. Environ. 113 (2009) S67–S77.
[62] U. Schreiber, T. Endo, H.L. Mi, K. Asada, Quenching analysis of chlorophyll fluorescence by the saturation pulse method — particular aspects relating to the study of eukaryotic algae and cyanobacteria, Plant Cell Physiol. 36 (1995) 873–882.
[63] S. Joshua, C.W. Mullineaux, Phycobilisome diffusion is required for light-state transitions in cyanobacterial, Plant Physiol. 135 (2004) 2112–2119.
[64] T. Ogawa, T. Harada, H. Ozaki, K. Sonoike, Disruption of the ndhF1 gene affects Chl fluorescence through state transition in the cyanobacterium synechocystis sp PCC 6803, resulting in apparent high efficiency of photosynthesis, Plant Cell Physiol. 54 (2013) 1164–1171.
[65] G. Tomita, E. Rabinowitch, Excitation energy transfer between pigments in photosynthetic cells, Biophys. J. 2 (1962) 483.
[66] J.F. Allen, Protein-phosphorylation in regulation of photosynthesis, Biochim. Biophys. Acta 1098 (1992) 275–335.
[67] B. Drop, M. Webber-Birungi, S.K.N. Yadav, A. Filipowicz-Szymanska, F. Fusetti, E.J. Boekema, R. Croce, Light-harvesting complex II (LHCII) and its supramolecular organization in *Chlamydomonas reinhardtii*, Biochim. Biophys. Acta Bioenerg. 1837 (2014) 63–72.
[68] S. Caffarri, T. Tibiletti, R.C. Jennings, S. Santabarbara, A comparison between plant photosystem I and photosystem II architecture and functioning, Curr. Protein Pept. Sci. 15 (2014) 296–331.
[69] G. Britton, UV/visible spectroscopy, in: G. Britton, S. Liaaen-Jensen, H. Pfander (Eds.), Carotenoids: Spectroscopy, Birkhauser, Basel 1995, pp. 13–62.
[70] B.H. Davies, H.P. Köst, Carotenoids, in: H.-.P Köst (Ed.), Handbook of Chromatography; Plant Pigments, CRC Press, Boca Raton 1988, pp. pp. 1–185.
[71] H.A. Frank, J.A. Bautista, J.S. Josue, A.J. Young, Mechanism of nonphotochemical quenching in green plants: energies of the lowest excited singlet states of violaxanthin and zeaxanthin, Biochemistry 39 (2000) 2831–2837.
[72] A.C. Ley, D.C. Mauzerall, Absolute absorption cross-sections for photosystem II and the minimum quantum requirement for photosynthesis in Chlorella vulgaris, Biochim. Biophys. Acta Bioenerg. 680 (1982) 95–106.
[73] M. Werst, Y. Jia, L. Mets, G.R. Fleming, Energy transfer and trapping in the photosystem I core antenna. A temperature study, Biophys. J. 61 (1992) 868.
[74] R.B. Peterson, E. Dolan, H.E. Calvert, B. Ke, Energy transfer from phycobiliproteins to photosystem I in vegetative cells and heterocysts of *Anabaena variabilis*, Biochim. Biophys. Acta Bioenerg. 634 (1981) 237–248.
[75] M. Watanabe, D.A. Semchonok, M.T. Webber-Birungi, S. Ehira, K. Kondo, R. Narikawa, M. Ohmori, E.J. Boekema, M. Ikeuchi, Attachment of phycobilisomes in an antenna–photosystem I supercomplex of cyanobacteria, Proc. Natl. Acad. Sci. 111 (2014) 2512–2517.
[76] G. Yamanaka, A. Glazer, Phycobiliproteins in Anabaena 7119 Heterocysts, Photosynthetic Prokaryotes: Cell Differentiation and Function, Elsevier Science Publishing, Amsterdam, 1983 69–90.
[77] B. Gobets, R. van Grondelle, Energy transfer and trapping in photosystem I, Biochim. Biophys. Acta Bioenerg. 1507 (2001) 80–99.
[78] A.M. Acuña, J.J. Snellenburg, M. Gwizdala, D. Kirilovsky, R. van Grondelle, I.H. van Stokkum, Resolving the contribution of the uncoupled phycobilisomes to cyanobacterial pulse-amplitude modulated (PAM) fluorometry signals, Photosynth. Res. (2015) 1–12.
[79] M. Toyoshima, N.V. Sasaki, M. Fujiwara, S. Ehira, M. Ohmori, N. Sato, Early candidacy for differentiation into heterocysts in the filamentous cyanobacterium Anabaena sp. PCC 7120, Arch. Microbiol. 192 (2010) 23–31.
[80] A.B. Juarez, L. Barsanti, V. Passarelli, V. Evangelista, N. Vesentini, V. Conforti, P. Gualtieri, In vivo microspectroscopy monitoring of chromium effects on the photosynthetic and photoreceptive apparatus of *Eudorina unicocca* and *Chlorella kessleri*, J. Environ. Monit. 10 (2008) 1313–1318.
[81] M.M. Saleh, D.N. Matorin, B.K. Zayadan, D.A. Todorenko, E.P. Lukashov, M.M. Gaballah, Differentiation between two strains of microalga *Parachlorella kessleri* using modern spectroscopic method, Bot. Stud. 55 (2014) 53.
[82] B. Osmond, O. Schwartz, B. Gunning, Photoinhibitory printing on leaves, visualised by chlorophyll fluorescence imaging and confocal microscopy, is due to diminished fluorescence from grana, Aust. J. Plant Physiol. 26 (1999) 717–724.
[83] H. Kupper, I. Setlik, M. Trtilek, L. Nedbal, A microscope for two-dimensional measurements of in vivo chlorophyll fluorescence kinetics using pulsed measuring radiation, continuous actinic radiation, and saturating flashes, Photosynthetica 38 (2000) 553–570.
[84] K. Oxborough, Using chlorophyll a fluorescence imaging to monitor photosynthetic performance, Chlorophyll a Fluorescence, Springer 2004, pp. 409–428.
[85] K. Omasa, A. Konishi, H. Tamura, F. Hosoi, 3D confocal laser scanning microscopy for the analysis of chlorophyll fluorescence parameters of chloroplasts in intact leaf tissues, Plant Cell Physiol. 50 (2009) 90–105.
[86] W.I. Gruszecki, K. Wojtowicz, Z. Krupa, K. Strzalka, A direct measurement of thermal-energy dissipation in the photosynthetic apparatus during induction of fluorescence, J. Photochem. Photobiol. B Biol. 22 (1994) 23–27.
[87] W.J. Vredenberg, A three-state model for energy trapping and chlorophyll fluorescence in photosystem II incorporating radical pair recombination, Biophys. J. 79 (2000) 26–38.
[88] W. Vredenberg, O. Prasil, On the polyphasic quenching kinetics of chlorophyll a fluorescence in algae after light pulses of variable length, Photosynth. Res. 117 (2013) 321–337.
[89] Y. Miloslavina, A. Wehner, P.H. Lambrev, E. Wientjes, M. Reus, G. Garab, R. Croce, A.R. Holzwarth, Far-red fluorescence: a direct spectroscopic marker for LHCII oligomer formation in non-photochemical quenching, FEBS Lett. 582 (2008) 3625–3631.
[90] S.B. Krumova, S.P. Laptenok, L. Kovács, T. Tóth, A. van Hoek, G. Garab, H. van Amerongen, Digalactosyl-diacylglycerol-deficiency lowers the thermal stability of thylakoid membranes, Photosynth. Res. 105 (2010) 229–242.
[91] J. Durrant, L. Giorgi, J. Barber, D. Klug, G. Porter, Characterisation of triplet states in isolated Photosystem II reaction centres: oxygen quenching as a mechanism for photodamage, Biochim. Biophys. Acta Bioenerg. 1017 (1990) 167–175.
[92] A. Telfer, Singlet oxygen production by PSII under light stress: mechanism, detection and the protective role of beta-carotene, Plant Cell Physiol. 55 (2014) 1216–1223.
[93] L. Zhang, T.B. Melo, H. Li, K.R. Naqvi, C. Yang, The inter-monomer interface of the major light-harvesting chlorophyll a/b complexes of photosystem II (LHCII) influences the chlorophyll triplet distribution, J. Plant Physiol. 171 (2014) 42–48.
[94] D.A. Hartzler, D.M. Niedzwiedzki, D.A. Bryant, R.E. Blankenship, Y. Pushkar, S. Sayikhin, Triplet excited state energies and phosphorescence spectra of (bacterio) chlorophylls, J. Phys. Chem. B 118 (2014) 7221–7232.